Dear Reviewers and Editor

We thank you all for your useful comments, which we have addressed below. Our responses are shown in blue text, while additions to or quotes from the manuscript are indicated by *italicised blue text*. Additionally, since the ACPD paper was submitted there has been a minor update to the photoacoustic data, which involves an update the way the background and microphone pressure sensitivity calculation was applied. Essentially rather than doing one fit per flight, an average fit for the whole dataset was used instead, with one fit for each wavelength. This has resulted in minor changes to some of the numbers for MAC and AAE but no change to the narrative or conclusions of the paper. Here is a summary of the changed numbers

	Old	New
Mean MAC 405nm	20.2 m^2g^{-1}	20.3 m^2g^{-1}
Mean MAC 514nm	14.5 m^2g^{-1}	14.6 m^2g^{-1}
Mean MAC 655nm	11.5 m^2g^{-1}	11.8 m^2g^{-1}
Mean $AAE_{405-514}$	1.39	1.38
Mean $AAE_{514-655}$	0.94	0.88
Mean $AAE_{405-655}$	1.16	1.13
Approx. Mean E_{Abs}	1.8	1.85
BrC absorption fraction 405nm	10%	11%
BrC MAC 405nm	0.27 m^2g^{-1}	0.31 m^2g^{-1}

We have also corrected an error in the caption to Figure 3 where the different panels were referred to incorrectly.

REVIEWER #1

Taylor et al. present in situ airborne measurements of BC mass, microphysical BC properties, and multi-wavelength absorption in aged smoke sampled off the coast of central Africa. The dataset analyses in terms of retrieving the effective MAC and com-pare several models of the absorption coating enhancement. This work is an important to constraining aerosol optical properties and evaluating parameterization that may be used to more accurately model the aerosol radiative effect, specifically black carbon. This work is high quality and appropriate for ACP and should be published with minor revisions.

Specific comments:

Although technically correct, is it necessary evaluate the absorption enhancement in a quasi-single particle manner? If one assumed a log normal BC SD and an average size independent coating thickness would calculation of Eabs be significantly different?

This has been recently investigated by Fierce et al. (2020) https://doi.org/10.1073/pnas.1919723117

We have added into 4.2

"We used a full 2-D bin scheme as absorption calculations using modal schemes, which assume a particular value of M_{BC} or MR, may show significant deviations from explicit calculations (Fierce et al. 2020)"

Please consider moving section S5 and figure S5 to the main text as it is an important piece of the main conclusions of this manuscript.

We have moved figure S5 to the main text as a new figure and incorporated the brief text into the caption.

Technical comments:

Page 5 line 33: Please add a reference describing the characterization of the rose-mount inlet.

We have added a reference to the Rosemount characterisation technical note.

Page 6 line 19: PCASP, for specific commercial instrumentation please state the model number and manufacturer

Done, but moved to section 2.2.

Page 11 line 5: Please explain why only level and straight legs were used? Was the data quality better?

We have added

"The use of straight and level runs allows us to have longer averaging times (typically 5 – 15 mins), minimising statistical uncertainties, as well as negating any possibly data misalignments due to different length sample lines."

Page 13 line 6: The last clause of this sentence is confusing and outplace. Please remove or edit it.

It now says

"One of the key features of these African smoke plumes is their long lifetime. After several days ageing in the tropical sun, visible absorption by BrC is dwarfed by absorption by BC."

Page15 line 25: This sentence is too broad. In the aged samples analyzed here, the BrC 'signal' is lower than the noise/uncertainty in the coating enhancement. However, in fresh smoke with the absorption dominated by BrC, it may be possible to extract a meaningful MAC of the OA.

We have clarified that this comment only refers to this dataset.

Page S5 line 1: Is this the same level flight leg used in the main text Fig 5? If so, please note it.

Noted.

Page S5, line 3: typo , 'correct'

It is now correct.

Page S11, line 20: References to the Dc distribution and Figure 5a should be update to reference figures in the manuscript.

This has been updated to Fig. S2a.

Figure 1: This figure is adequate but could be used to tell more of the story. Consider adding the approximate fire locations and arrows indicating the transport direction and time.

These have been added to Figure 1.

Figure 5: Please consider added a mirrored axis on top with the spherical equ. diameter. Are other legs similar to this example? Is MR size dependent for all of the analyzed legs. Please add a sentence to the text describing the variably of this plot for the whole dataset

We have added in the mirror axes and change the caption accordingly. We've also added

"Equivalent distributions were generated for each straight and level run during the campaign, and the broad features were similar across all the distributions showing biomass burning aerosol"

All the biomass burning distributions looked very similar on visual inspection. As a sanity-check we had a look at emissions from the diesel ground power unit when on the ground, and this showed just thinly coated particles across all sizes.

REVIEWER #2

This study presented black carbon (BC) microphysical properties and aerosol absorption over the southeast Atlantic Ocean during the CLARFY-2017 aircraft campaign. The authors showed that BC particles have high values of mass absorption coefficient (MAC) (~20 and~15 m2 g-1 at the wavelength of 405 and 514 nm, respectively) and absorption enhancements (~1.8) during the campaign, and these results suggest the importance of the lensing effect by coating species. The contribution of brown carbon (BrC) was estimated to be~10% from observed absorption Angstrom exponents (AAE) at three wavelengths. The authors also made an absorption closure analysis through the comparisons of the observed MAC and AAE values with the calculated values using the Mie theory and empirical parameterizations. The authors clearly showed that the calculations by the Mie theory (homogeneous grey mixture and core-shell assumption) cannot reproduce all the observed features of MAC and AAE, while they are reproduced reasonably well by some empirical parameterizations.

The scope of this manuscript is will suited to ACP. The topic of this study is very interesting because the accurate understanding on the microphysical and optical properties of BC particles is key to improve our estimation of aerosol impacts on the global climate. The manuscript is written very well, and the uncertainties and implications of the data are discussed in detail. This manuscript should be published by ACP after revising some minor points.

Minor comments:

1) Page 1, Lines 3-4: Highly aged biomass burning plumes The information of "4-8 days from sources" may be useful for readers.

We have added this information.

2) Page 1, Line 12: MAC of BC I suggest to add the values of BC MAC here (at least for the visible wavelength).

We have added these values to the abstract.

3) Page 2, Line 18:I think 40% is too high. CMIP6 emissions (for the year 2010) are~10 Tg y-1 for total BC and~8 Tg y-1 for anthropogenic BC.

We have changed this to *"open biomass burning is a major source of global BC emissions".*

4) Page 4, Lines 9-13:These sentences describe what the authors did in the manuscript. I think the authors can clarify the objectives of this study here (e.g., investigate the absorption closure between microphysical and optical properties of BC for highly-aged biomass burning plumes).

This now says

"We quantify the range of values of measured MAC and AAE and investigate the absorption closure between microphysical and optical properties of BC for highly-aged biomass burning plumes."

5) Page 4, Section 2.2:Please provide the particle size ranges observed by the SP2 and PAS. The SP2 could measure most BC particles in the atmosphere? The size range of SP2 is

consistent with that of PAS? Their difference can affect the results and conclusions of this study?

We have added in to section 2.2:

"For BC mass measurements, the SP2 detection limits are driven by a gradual drop-off in detection efficiency for particles with BC content less than around 1 fg (102 nm mass-equivalent core diameter (D_C) (Schwarz et al., 2010), and a sharp cut-off at 143 fg (533 nm equivalent D_C), where the incandescence detector saturates. For particles that saturate the incandescence detector, we assume the BC content is 143 fg. Particles with BC content less than 1 fg are numerous but contain a negligible fraction of the total BC mass. Particles larger than 143 fg BC are rare, and by examining lognormal fits to the BC mass distribution, we estimate the uncertainty in the BC mass concentration caused by detector saturation is less than 1%. The SP2's upper cut-off diameter in terms of total particle diameter (D_P, i.e. the coated diameter for coated particles) is not affected by detector saturation in any practical sense, and is determined by aerodynamic limitations of particles entering the inlet, and is likely to be in the region of 1 µm. The instrument inlets are discussed further below."

We had already stated later in Section 2.2 that the PAS samples behind a 1.3µm impactor. We now discuss a few paragraphs later the slightly different cutoff diameters of the various instruments:

"The inboard aerosol instruments all sampled from Rosemount inlets, and the instrumental setup and detection ranges mean they all sampled a comparable size range of accumulation mode submicron aerosol (Trembath et al., 2012). The main instruments discussed here have slightly different upper cut-off diameters; 1.3 µm for the PAS, 1 µm for the AMS, and around 1 µm for the SP2. Wu et al. (2020) presents aerosol size distributions measured at ambient humidity using a passive cavity aerosol spectrometer probe (PCASP, Droplet Measurement Technologies, model SSP-200). Examination of these size distributions determined that the difference between a cut-off of 1.0 and 1.3 µm equated to 1.5% in terms of the total particle volume distribution."

6) Page 4, Lines 12-18:Please clarify how AMS and CO data were used in this study.

We've clarified that

"The AMS data are used to provide some context to the black carbon and optical measurements, as well as to calculate the density of the non-BC components. An in-depth discussion of the aerosol chemical composition and vertical profile is presented by Wu et al (2020)"

and

"The CO data are used as a measure of the amount of pollution throughout the atmospheric profile."

7) Page 6, Line 7:Delete "to".

Done.

8) Page 7, Line 6:Kondo et al. (2011), which showed MMD for biomass burning plumes, can be cited here.

Done.

9) Page 7, Line 25: The ratio of observed MAC to the values by Bond and Bergstrom(2006)I think the uncertainty in the values by Bond and Bergstrom (2006) should be considered in the Eabs estimation (1.8±“uncertainty” is better).

We have added in uncertainties to E_{Abs} throughout the paper, these are now all 1.85 +/- 0.45.

10) Page 7, Lines 22-28:Please add MAC values at the three wavelengths to this (or related) paragraph. I think MAC values themselves are important.

We have added in the average values and uncertainties to this section.

11) Page 8, Lines 6-7:The particles size ranges are consistent between SP2 and AMS? This should be considered in the uncertainty in OA MAC.

We have added in to the AMS description:

“The AMS detection size range is determined by the transmission of the aerodynamic lens on the instrument's inlet, which has transmission efficiency near 100\% over the size range 50 – 1000 nm (Liu et al. 2007).”

Pleas also see the previous comment about the size ranges of the PAS and SP2.

12) Section 3: The authors should note the importance of aerosol water to MAC and Eabs in this or discussion section. The values in this study are for dry conditions, but MAC and Eabs in the real atmosphere (ambient RH) are important in evaluating their climate impacts.

We have added to the end of section 5.1:

It is important to note that all our measurements took place at dry humidities, and our modelling did not include the effects of aerosol water. Haslett et al. (2019) used a core/shell Mie model to calculate that in aged plumes measured over southern West Africa, the condensation of water at relative humidities up to 98% at the top of an aerosol layer could cause the aerosol optical depth to increase by a factor of over 1.8. Experimental studies of absorption at these high humidities are rare, though Brem et al. (2012) observed that absorption of OM generated by wood pyrolysis increased by over a factor of 2 as the RH increased from 32% to 95%, where scattering only increased by a factor of ~1.4. However, there was little change in absorption at humidities below 80%, and both absorption and scattering showed steep rises at RH greater than 90%. In our dataset these humidities were not reached throughout the bulk of the aerosol plume in the atmospheric column, as shown in Fig. 2, but they were sometimes observed in clear-sky conditions near the top of the boundary layer. The effects of high relative humidity on aerosol absorption are poorly constrained, and although we are not able to provide any further constraint from our measurements, we recommend further study on this topic.

13) Page 8, Lines 31-32: It is better to describe the optical models and parameterizations used in this study briefly in the main text.

We have added some extra to the main text, so this now says

"The optical models and parametrisations tested in this analysis are listed in Table 1, and described in detail in supplementary Sect. S1. We have tested the core/shell Mie model, as well as several homogeneous grey sphere models, which utilize a Mie model with a sphere of one single complex refractive index, calculated using different rules to account for the mixing between BC and non-BC components. The different mixing rules are: (i) volume mixing, where the refractive index is averaged weighted by the volume of each component; (ii) Maxwell-Garnett approximation (Markel, 2016), which considers mixing of small particles of BC dispersed throughout a non-BC host medium; and the Bruggeman mixing rule (Markel, 2016), which computes the refractive index of two components dispersed evenly within a particle. We have also tested several parametrisations of either MAC or E_{Abs} (Liu et al., 2017; Chakrabarty and Heinson, 2018; Wu et al., 2018), which are based on empirical or semi-empirical fits to MAC or E_{Abs} for particles with different mixing states using real and/or modelled particle data."

14) Page 9, Lines 14-23:This part (steps 1-6) is not easy to understand. How about adding a figure to explain this process?

We have added a new figure to the supplementary section (Figure S2) showing a schematic of the SP2 mass distribution processing, while we refer the reader to this schematic in the main text.

a) Please clarify steps 1-2 are theoretical calculations and steps 3-6 use observed data.

We have clarified in the text that *"Steps 1 and 2 are purely theoretical calculations, whereas steps 3 -- 6 involve processing of the measured data."*

b) Please explain what is the Liu et al. correction.

We have added information concerning the Liu et al correction *"This empirical correction to the core/shell Mie model accounts for the fact that particles with MR < 3 do not scatter light at 1064nm exactly as described by the core/shell Mie model".*

c) The spherical-equivalent core in step 4 is the same as the spherical-equivalent DBC in step 3? Step 4 is to calculate shell diameter only?

Yes, we have rephrased this as:

"Process single-particle data through the table to calculate the single-particle spherical-equivalent shell diameters, including the Liu et al. correction".

d) "Convert the single-particle data to equivalent MBC and MR": I think MBC is calculated in step 3. So, step 5 is to calculate MR?

Yes, we have rephrased this step

"Convert the single-particle shell/core ratio to MR and bin the data into a 2-D distribution of MR vs M_{BC}".

e) Step 6: this is not easy to understand unless readers read SI.

We have added in a reference to supplementary S2.

15) Page 10, Lines 9-12:This part should be explained near the explanation of the 6 steps.

We have added an explanation of the Liu et al correction into step 2.

16) Page 11, Line 19:The core/shell Mie model (green lines in Figs 6 and 7)

Done.

17) Page 11, Line 30:Please explain briefly what is the “skin depth effect” here (though they are described in SI). Some papers should be cited.

We have added in *“the skin depth effect prevents light interacting fully with all the light absorbing BC, as the surface of the sphere absorbs and scatters light and shields the centre, which is then less effective at absorption (Wang et al, 2015).”* We have also referenced Chakrabarty et al (2018) a few sentences later in the same paragraph.

18) Page 12, Lines 8-10:I suggest the authors to add observed AAE for BC only to Fig 7a and 7c (like Fig 6aand 6d).

Done.

19) Page 12, Lines 11-12:Is it not possible to show the kBC dependency of MAC and AAE for the parameterizations? Please explain why the results are shown at a kBC value for each parameteri-zation.

The parameterisations developed previously by others were for specific values of $\boldsymbol{m}_{BC}$, and thus they do not enable predictions with varying $\boldsymbol{m}_{BC}$. We have edited the figure caption to explain why:

“Panels (a) -- (c) show different Mie models evaluated at various values of $\boldsymbol{m}_{BC}$, plotted against k_{BC} on the horizontal axis. Panels (d) -- (f) show parametrisations which are plotted at the values of k_{BC} at which the parametrisations were developed.”

20) Page 15, Line 32:RI should be changed to refractive index.

Done.

21) Text S2, Line 3:do not “correct”.

Done.

REVIEWER #3

The authors have investigated the optical properties of black carbon (BC) and organic carbon from highly aged biomass burning plumes as part of the CLARIFY-2017 field campaign. They measure the mixing state of BC using an SP2, and the optical proper-ties using photoacoustic spectroscopy. They use these measurements to obtain MAC, MAC enhancement, and AAE values for the aged biomass burning aerosol. These measurements are then compared to several different models for calculating biomass burning optical properties. These include coated sphere models, homogeneous grey sphere models, and more complicated aerosol optical models that account for aerosol morphology (semi-empirical models). These measurements also allow for an estimation of the contribution of brown carbon aerosol to overall absorption in aged biomass burning aerosols (10% at 405 nm). The authors conclude that all models are sensitive to the choice of refractive index for BC. The authors also conclude that Mie models be implemented with great caution when calculating aerosol optical properties.

Major comments:

1) The authors rely heavily on SP2 measurements for most of their analysis. It would be helpful to comment on potential effects of charring of organics in the SP2 as detailed in Sedlacek et al. 2018 (Aerosol Research Letters 52:15, 1345-1350) and if these would affect any of the measurements detailed here.

We have added to the experimental section

"Under certain conditions, charring can occur as weakly absorbing particles enter the SP2's laser, causing a false black carbon signal. Sedlacek et al. (2019) showed this can occur for fulvic and humic acids (BrC surrogates), but only when they had been passed through an external heated tube furnace, which we do not use in our experiment. Artificial tar balls formed through anoxic pyrolysis may also show a false rBC signal, but tar balls formed in real fires have been observed to show no detectable incandescence signal in the SP2 (Adler et al, 2019). We therefore do not consider this to be a major concern for our observations."

2) p 14. line 12-22: The authors describe alternatives to the lensing effect of MAC and mention the possibility of externally mixed intermediate absorbers (IA) affecting total particle absorption and demonstrate that the resulting calculations do not match their observations. If possible, could the authors perform similar calculations for IA internally mixed with BC and show if such a scenario matches the values observed here. An internal mixture of IA and BC would reduce the BC MAC while also reducing the resultant AAE.

The calculations suggested by the reviewer are not easy to perform. Firstly, we would need to know the wavelength-dependence of the IA refractive index, which is currently unknown. We would also find that the answer would strongly depend on which model was used to calculate the optical properties of the internally mixed particles. For example, see our response to Dr Lewis et al. below and the new Table 2, which show large model-to-model variability even without the presence of an IA or BrC. Our absorption spectrum is only 11% different at 405nm from what we might expect from pure BC, so it is unlikely that IA can have a strong effect if they have AAE anything like those in literature.

3) The main critique I have of this paper is that they provide too little detail on what makes each optical model unique. It is good that they are verifying different optical models with real world data, but one needs to be familiar with the models used for it to make sense why they give different results. I believe a little more explanation is warranted.

The reviewer raises a good point, which was also raised by Reviewer 2. We refer the reader to our response to comment #13 by Reviewer 2.

4) The semi-empirical models all matched the measured AAE well, and MAC values calculated using Chakrabarty and Heinson method and the Liu method matched the measured values well. MAC enhancement predicted using Liu's method matched MAC enhancement values the closest, but it is unclear why the Chakrabarty MAC enhancement did not, as they are very similar techniques. The authors reason that the enhancement calculated using the Chakrabarty and Liu methods give different results but are similar methods. The authors speculate that this has to do with morphology ,did they collect any samples to image the particle morphologies?

The reviewer is right to highlight our assertion that morphology may be responsible for the small differences in the predicted MAC values from the parameterisations of either Chakrabarty and Heinson (2018) or Wu et al. (2018). However, we only suggested the role of morphology as a possibility and it is beyond the scope of this paper to investigate differences in the specific simulations examined by these two previous studies. We have amended our discussion in Sect. 5.2 to read:

"We speculate that it may either be related to some detail of the morphology of the particles used in their simulations, or some particular details of the optical models or refractive indices used, but it is beyond the scope of this paper to make in-depth comparisons of simulations from literature."

5) Overall, the paper is well written but is a bit lengthy. I think perhaps the finer details in sections 4 and 4.1 could be shortened or relegated to the SI.

A lot of section 4 started off as a big supplement but several coauthors responded saying they were not familiar with the SP2 technique and didn't understand what was going on. With this in mind we have decided to leave it as is. Indeed, the SP2 analysis applied in this work is significantly different to that ordinarily applied by many others who have reported SP2 mixing state analyses (e.g. the Liu et al correction).

Other comments:

1. Section 2.2: Are there any limitations or artifacts in the instrumentation that should be mentioned or accounted for?

We have tried to incorporate these into the listed uncertainties. We have also added in the detection limits in response to reviewer #2.

2. Figure 3: Should error in the MAC of BC as reported by Bond and Bergstrom account for error?

We have added to the figure caption:

"The uncertainties in the average values are ±19% for MAC and ±25% for E_{Abs}."

We have added into the instrumental section about the uncertainty in E_{Abs}:

"We also calculate E_{Abs} by dividing the measured MAC by the values reported for fresh BC by Bond and Bergstrom (2006) of 7.5±1.2 m^2g^{-1} at a wavelength of 550 nm. The uncertainty in E_{Abs} is then 25%, calculated by combining the uncertainty in our measured MAC with the range of MAC from Bond and Bergstrom (2006)."

3. p. 6, line 1: Were checks put on the upper limit of the SP2 measurements as high BC concentrations can be underestimated by the instrument, or were concentrations below the upper limit of the SP2 measurement range throughout the campaign?

The reviewer raised a good point, we have added the following clarification to Sect. 2.2

"The SP2 single-particle data were also examined for coincidence at high concentrations, which would cause the instrument to undercount the BC number and mass concentrations. The highest BC number concentrations measured were just below 1000cm^{-3}, and with this high loading 2% of particle detection windows showed coincident particles. To correct for this small bias, the coincident particles were included in the concentrations of BC mass and number concentrations, but not in the single-particle mixing state analysis, as the leading edge scattering signal can only be measured for the first particle in a measurement window."

To be clear, the BC mass and number concentrations have not been revised since the previous version, the coincident particles were already included in the concentrations.

4. p. 8, line 8: As the OA absorption is calculated by subtracting total absorption by extrapolated BC absorption, the uncertainty propagation would also need to account for uncertainties in BC absorption measurements.

The BC concentration drops out of the calculation, like it does for the fraction of BrC absorption. To make this clearer we have defined the equations for both of these on pages 8 & 9 in Section 3, and explicitly stated that the BC concentration drops out.

5. Page 8: add details about optical models

We have now done this. Again, please see our response to comment #13 from Reviewer #2 for further details.

6. Page 9: I think the 6 step outline is going to be confusing for some, I would con-sider rewriting to make it more clear what is a measurement and what is a theoretical calculation

We have added the following clarification:

"Steps 1 and 2 are purely theoretical calculations, whereas steps 3 – 6 involve processing of the measured data."

Please also see our responses to reviewer 2, points 14 (a) to (e), where we have gone into more detail and included a schematic figure of the whole process.

7. Page 10: There is some explanation of the Liu correction that should be moved to an earlier spot in the text

We have included more detail in step 2

"This empirical correction to the core/shell Mie model accounts for the fact that particles with MR < 3 do not scatter light at 1064 nm exactly as described by the core/shell Mie model"

8. p 11. line 24: typo "experimental" written twice

Done.

9. p 13. line 21: It would be better to quantify the coating rather than just stating the particles to be thickly coated.

We have moved a later statement to the location the reviewer highlights to clearly communicate the thickness of the coating:

"The BC particles measured during CLARIFY were universally thickly coated, with median MR values in the range 8 – 12".

10. p 16. line 11: The line reads as if BC acts as the coating material and I think that is not the intended meaning here. Please edit the sentence to make it clear.

This now says *"coatings on BC-containing particles".*

Ernie Lewis et al.

In their manuscript, Taylor et al. conclude that the contribution to aerosol light absorption at 405 nm by brown carbon (BrC) is roughly 10%, as inferred from the difference in the measured light absorption at that wavelength and the value extrapolated from measurements at 514 and 655 nm together with the assumption that the absorption due to black carbon (BC) over all three of these wavelengths is inversely proportional to the wavelength. We wish to point out that this is not necessarily a valid assumption. We are not suggesting that they did not measure absorption from BrC (which they discuss in more detail later in their manuscript), but merely want to state that the absorption from black carbon particles is not always inversely proportional to the wavelength; or, alternatively, that the absorption Angstrom exponent (AAE) for BC is not exactly equal to unity.

To demonstrate that this is the case, we calculated (see Fig. 1) the AAE for the 405-514 nm and the 514-655 nm wavelength pairs for monodisperse aerosols of pure BC spheres, using the index of refraction used by Taylor et al. (2.26-1.26i). The AAE for the 405-514 nm pair increases from 1.0 for very small diameters (<~20 nm) up to a maximum of 1.54 for 80 nm diameter particles, after which it decreases to 1.43 for100 nm diameter particles, 0.2 for 150 nm diameter particles, and -0.19 for 200 nm diameter particles, remaining below zero for larger ones. The behavior of the 514-655nm AAE is similar, but the diameters are shifted to larger values. For diameters lessthan~90 nm, the AAE for the 405-514 nm pair is greater than that for the 514-655 nm pair, and the argument of Taylor et al. would attribute some of the BC absorption at405 nm to BrC. Similarly, for diameters greater than~90 nm, there would be a deficit of absorption at 405 nm.

For BC particles with associated substances (commonly referred to as coatings) the situation is perhaps more extreme. We also performed calculations for BC coated with a nonabsorbing coating in a concentric core-shell configuration, using 1.5-0i for the index of refraction of the coating, a BC core mass-equivalent diameter of 100 nm (corresponding to a mass of 0.94 fg), and a coating:core mass ratio of 20 (corresponding to a coating thickness of 104 nm, using a core density of 1.8 g/cmˆ3 and a coating density of 1.3 g/cmˆ3). Such particles are in the center of the hot spot of their 2-Ddistribution shown in Fig. 5 of their manuscript. For such a large coating:core mass ratio the assumption that a core-shell configuration accurately yields the absorption of the particle seems not unreasonable. The AAE for the 405-514 nm wavelength pair is0.49, whereas that for the 514-655 pair is 1.53, neither of which is near unity. Further-more, extrapolation of the latter AAE to 405 nm would result in less absorption than measured.

We realize that BC particles are not spheres, and perhaps not concentric core-shell configurations, and certainly not monodisperse. However, the assumption that the AAE is identically unity for BC absorption, which is the premise of one of the arguments made by Taylor et al. to infer BrC absorption, is not necessarily true.

Ernie R. Lewis, Brookhaven National Laboratory; Arthur J. Sedlacek III, Brookhaven National Laboratory; Timothy B. Onasch, Aerodyne Research Incorporated

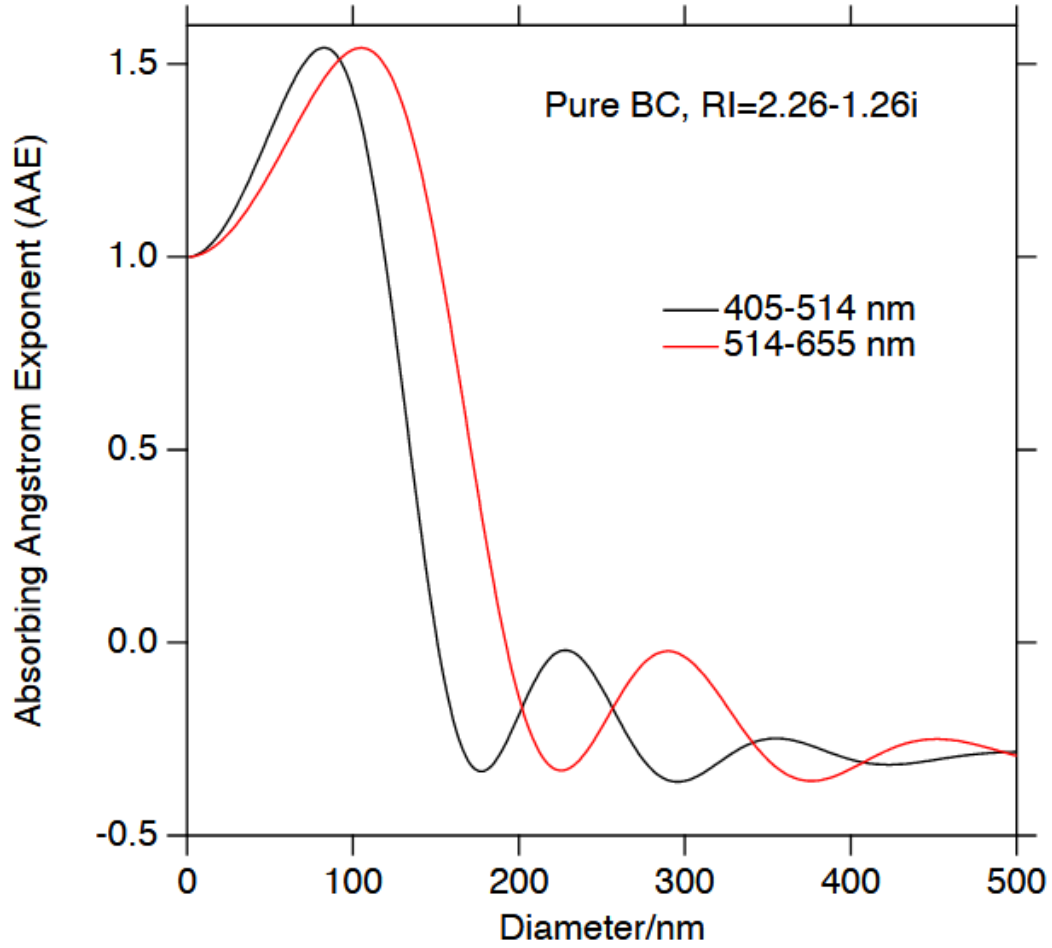

Fig. 1.absorbing Angstrom exponent of pure black carbon spheres

We thank Dr Lewis and co-commenters for their useful thoughts on our manuscript. Their concern relates to our Fig. 4 where we extrapolate the measured AAE between 514-655nm (previously 0.94, now 0.88, not unity as they state) to shorter wavelengths and use this to deduce the BrC absorption fraction at 405nm. They give some monodisperse Mie calculations that show very different AAE values to our empirical measurements in both wavelength ranges. We acknowledge that their concerns are valid, however their illustrative approach gives more extreme results than a full consideration of the BC size distribution. Firstly, when integrating the full polydisperse BC size distribution, the average AAE values settle at some average value between the extreme values they show, and this is not necessarily in the same location as the AAE of the mass or number median diameters. Secondly, when using a Mie model, particularly with a high BC refractive index, the strong skin-depth shielding effect may give low AAE values that are not observed in real particles, which are not perfectly spherical. Dr Lewis and co-commentators state that “For such a large coating:core mass ratio the assumption that a core-shell configuration accurately yields the absorption of the particle seems not unreasonable”, however our results in Figure 7 show that for calculations involving AAE the core/shell Mie model does produce results that do not agree with our observations.

We re-plotted Figure 4 to estimate the BrC absorption fraction at 405 nm, but instead of using the measured $AAE_{514\text{-}655}$ to extrapolate the 655nm MAC to shorter wavelengths, we used the AAE values from the different optical models.

These are the corresponding calculated BrC absorption fractions at 405 nm:

"Table 2. BrC absorption fraction at 405 nm calculated empirically or using the AAE from optical models. The minimum, mean, and maximum refer to the range of results from using the different values of $\boldsymbol{m}_{BC}$ *.*

Model	*Min*	*Mean*	*Max*
Core/shell	*23*	*26*	*33*
Bruggeman	*13*	*15*	*21*
Maxwell-Garnett	*13*	*15*	*20*
Volume mixing	*13*	*16*	*23*
Chak-MAC	*-*	*6*	*-*
Observations	*-*	*11 +/- 2*	*-*

"

We have added a short subsection as a new section 4.3

"In the calculations shown in Sect. 3 and Fig. 4, we presented an estimate of the fraction of absorption at 405 nm that was due to the presence of BrC, not BC. This estimate relied on the assumption that the AAE of BC was invariant with wavelength within the visible spectrum. Mie models predict that the AAE of BC is highly dependent on the size of the particles (Lack and Cappa, 2010). When considering a polydisperse BC size distribution, much of this variability will average out, however we conducted some additional calculations to test the robustness of our empirical estimate. The MAC of BC at 405 nm was re-calculated by extrapolating the measured MAC at 655 nm, using the AAE provided by the optical models described earlier in this section, with the full 2-D mixing state of the BC-containing particles. By using only the models' wavelength dependence of absorption, this approach accounts for the over- or under-prediction of the MAC of BC at the longer wavelengths, which would otherwise have a large effect on the calculated BrC absorption fraction. As in Fig. 4, any absorption in excess to this extrapolation is ascribed to BrC. The results of these calculations are shown in Table 2. The model results were broadly consistent with our empirical calculation in that they showed that the large majority of absorption was due to BC at this short wavelength. The model-to-model variability was large, and similar in size to the calculated BrC absorption fraction."

For reference here is the equivalent of figure 4, with the model estimates put on, but we have not included this in the revised manuscript as it looks messy and is better summarised in the table.

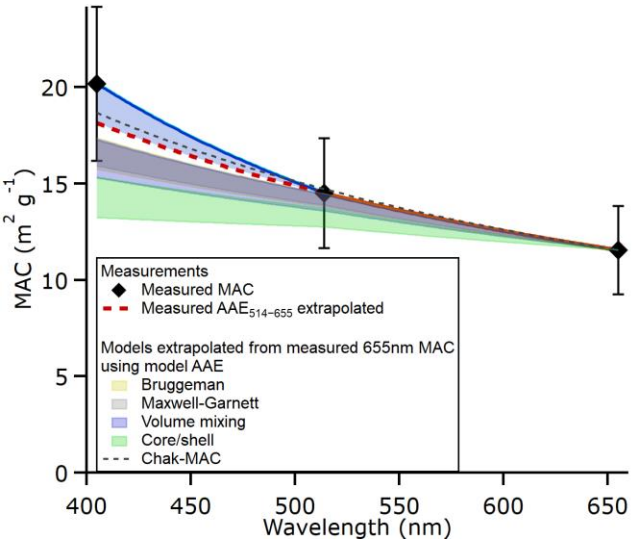
MAC (m^2 g^{-1})
20
15
10
5
0
400
450
500
550
600
650
Wavelength (nm)
Measurements
Measured MAC
Measured AAE$_{514-655}$ extrapolated
Models extrapolated from measured 655nm MAC using model AAE
Bruggeman
Maxwell-Garnett
Volume mixing
Core/shell
Chak-MAC

Absorption closure in highly aged biomass burning smoke

Jonathan W. Taylor[1], Huihui Wu[1], Kate Szpek[3], Keith Bower[1], Ian Crawford[1], Michael J. Flynn[1], Paul I. Williams[1,2], James Dorsey[1,2], Justin M. Langridge[3], Michael I. Cotterell[4,*], Cathryn Fox[3], Nicholas W. Davies[3], Jim M. Haywood[3,4], and Hugh Coe[1]

[1]Centre for Atmospheric Science, Department of Earth and Environmental Sciences, University of Manchester, United Kingdom
[2]National Centre for Atmospheric Science, University of Manchester, United Kingdom
[3]Met Office, Exeter, United Kingdom
[4]College for Engineering, Mathematics and Physical Sciences, University of Exeter, Exeter, United Kingdom
[*]Now at School of Chemistry, University of Bristol, Bristol, United Kingdom

Correspondence: Jonathan Taylor (jonathan.taylor@manchester.ac.uk)

Abstract. The optical properties of black carbon (BC) are a major source of uncertainty in regional and global climate studies. In the past, detailed investigation of BC absorption has been hampered by systematic biases in the measurement instrumentation. We present airborne measurements of aerosol absorption and black carbon microphysical properties in highly aged biomass burning plumes measured 4 – 8 days from source over the southeast Atlantic ocean during CLARIFY-2017, using a suite of novel photoacoustic spectrometers to measure aerosol absorption at 405 nm, 514 nm, and 655 nm, and a single-particle soot photometer to measure the BC mass concentration, size, and mixing state. These measurements are of sufficient quality and detail to provide constraint on optical schemes used in climate models for the first time in biomass burning plumes far from source, an aerosol environment that is one of the most important climatically.

The average absorption Angstrom exponents (AAE) were ~~1.39~~ 1.38 over the wavelength range 405 – 514 nm, and ~~0.94~~ 0.88 over the range 514 – 655 nm, suggesting brown carbon (BrC) contributed to ~~10~~ 11 ± 2% of absorption at 405 nm. The effective OA mass absorption coefficient (MAC) was ~~0.27~~0.31 ± ~~0.08~~0.09 $\mathrm{m^2\,g^{-1}}$ at 405 nm. The BC particles were universally thickly-coated, and almost no externally-mixed BC particles were detected. The average MAC of BC was ~~also high,~~ 20 ± 4 $\mathrm{m^2g^{-1}}$, $15\pm3\mathrm{m^2g^{-1}}$, and $12\pm2\mathrm{m^2g^{-1}}$ at wavelengths of 405 nm, 514 nm, and 655 nm respectively, with equivalent absorption enhancements of around ~~1.8~~ 1.85 ± 0.45 at all three wavelengths, suggesting that the thick coatings acted as a lens that enhanced light absorption by the BC.

We compared the measured MAC and AAE values with those calculated using several optical models and absorption parametrisations that took the measured BC mass and mixing state as inputs. Homogeneous grey sphere Mie models were only able to replicate MAC for some low (real and imaginary) values of the complex BC refractive index ($\boldsymbol{m}_{\mathrm{BC}}$) at the shortest wavelength, but they would have to use unrealistically low values of $\boldsymbol{m}_{\mathrm{BC}}$ to accurately replicate AAE. A core/shell Mie model was able to generate good agreement for MAC in the green/red end of the visible spectrum for most values of $\boldsymbol{m}_{\mathrm{BC}}$. However, there are no possible values of $\boldsymbol{m}_{\mathrm{BC}}$ that produce MAC values that agree with our observations at all three wavelengths, due to a wavelength-dependent underestimation of the MAC of the underlying BC core. Four semi-empirical parametrisations from literature were also tested, linking BC mixing state to either MAC or absorption enhancement. Two of these schemes produced

results that agreed within a few percent of the measured MAC at all three wavelengths, and AAE agreed well when discounting the effects of BrC.

Our results uniquely demonstrate the validity of absorption parametrisations, as well as the failings of Mie calculations, in this highly aged environment. We recommend future work should conduct similar analyses in environments where BC has different properties, and investigate the impact of implementing these types of schemes within climate models, as well as developing equivalent schemes for light scattering by soot particles at visible wavelengths.

1 Introduction

Every year, vast plumes of smoke are lofted into the free troposphere by open biomass burning in central and southern Africa. These plumes make their way westward over the ocean, and have an important effect on the radiative budget over the southeast Atlantic. Near the African continent, a stratocumulus deck sits atop the boundary layer, presenting a high-albedo surface that reflects solar radiation. Further west, the boundary layer deepens and the cloud deck becomes more broken, revealing the low-albedo sea surface below. Over cloud, the presence of absorbing aerosol in the free troposphere lowers the planetary albedo, but can potentially thicken the cloud deck by warming the free troposphere and strengthening the trade inversion (Wilcox, 2010). Smoke is also entrained into the boundary layer, where it increases concentrations of cloud condensation nuclei (CCN), brightening the clouds and raising their albedo, but this entrainment may also reduce cloud cover by warming the boundary layer and weakening the inversion (Zhang and Zuidema, 2019). These counterbalancing effects are all sensitive to the properties of the aerosol, and the radiative effects are particularly sensitive to the aerosol optical properties. More absorbing aerosol could change the sign of the associated radiative forcing for the semi-direct effect from negative to positive (Zhou et al., 2017).

Black carbon (BC) aerosol is the main absorbing component in these smoke plumes, and is a major climate warming agent globally. Open biomass burning is ~~responsible for around 40% of all~~ a major source of global BC emissions, and African fires make up around 40% of all open burning (Bond et al., 2013). The mass absorption coefficient (MAC, the ratio of absorption cross-section to BC particle mass) is the key variable for characterising the absorbing properties of BC. The MAC of fresh, uncoated BC is relatively well constrained; Bond and Bergstrom (2006) summarised measurements and found the MAC of uncoated BC to be $7.5 \pm 1.2\ \mathrm{m^2\,g^{-1}}$ at a wavelength of $550\ \mathrm{nm}$, with a wavelength-dependence that can be accurately described using an absorption Angstrom exponent (AAE) of 1. To date this work remains the most comprehensive summary of the MAC of fresh soot, and scientific effort since then has mostly focused on the modification of BC's absorbing properties by non-BC species such as organic aerosol (OA) and inorganic salts (e.g. Liu et al., 2017), as well as absorption by brown carbon (BrC) (e.g. Forrister et al., 2015; Healy et al., 2015). Where BC is encapsulated by non-BC material, the MAC of the soot may increase by a lensing effect, which is often quantified using absorption enhancement (E_{Abs}, the ratio of the absorption of coated BC to that of uncoated BC). In biomass burning plumes, BC demonstrates some internal mixing in the first few hours after emission (Akagi et al., 2012), but the effects of this mixing in terms of optical properties remain poorly quantified over timescales of both hours and days.

The core/shell Mie model considers encapsulated BC as two concentric spheres, and predicts thickly coated particles can have absorption enhanced by a factor of 2 – 3 (Bond et al., 2006). However, E_{Abs} values in this range have almost exclusively been measured where particles have been artificially aged (Schnaiter et al., 2005; Mikhailov et al., 2006; Peng et al., 2016), and have not generally been found in atmospheric measurements. Several studies have shown that using the Mie core/shell model can overestimate E_{Abs} (e.g. Cappa et al., 2012; Healy et al., 2015). Liu et al. (2017) summarised measurements of variable ageing of diesel emissions in western nations and showed that E_{Abs} was generally below 1.5. However, subsequent measurements have found E_{Abs} up to 2 in aged pollution in Beijing in both summer and winter (Xie et al., 2019a, b). Comparisons to Mie models are complicated due to size-dependent underprediction of the MAC of bare soot at shorter visible wavelengths, size-dependent overestimation of E_{Abs}, and only a moderate level of constraint on the BC refractive index (Bond and Bergstrom, 2006).

The addition of coatings may also cause fractal soot aggregates to collapse into a quasi-spherical shape, and Li et al. (2003) observed compacted soot particles using transmission electron microscopy on samples of aged haze from biomass burning in southern Africa. This could reduce absorption as less of the soot is exposed to the light (Scarnato et al., 2013), or increase absorption due to stronger interactions between neighbouring soot spherules (Liu et al., 2008). The relative importance of these two competing effects is wavelength-dependent in complex optical models, but experimental evidence of either effect remains sparse.

BrC is another major absorbing component of combustion aerosol, and this can include absorption by an emerging classification type for BrC referred to as tar balls. Primary emissions of BrC are particularly prevalent in biomass burning smoke, and secondary BrC may form photochemically or by condensation as plumes cool. BrC absorbs strongly at shorter visible wavelengths, but has a higher AAE than BC (typically greater than 2), and is not a strong absorber at longer visible wavelengths (Lund Myhre and Nielsen, 2004). This means that AAE may be used to discriminate between the relative contributions of BrC and BC to total absorption. Primary BrC becomes less absorbing with time due to photochemical bleaching. The majority of BrC absorption decays with a half-life in the region of 9 – 15 hr (Lee et al., 2014; Forrister et al., 2015), but laboratory studies have shown that some BrC species are particularly resistant to some bleaching pathways, such as reactions with ozone (Browne et al., 2019). Moreover, aged biomass burning aerosol may also have a significant BrC component arising from consistent mechanisms acting towards secondary BrC formation over the aerosol atmospheric lifetime.

In climate models, optical property schemes are chosen based on simplicity of implementation and computational efficiency. Schemes based on Mie theory are relatively simple to implement, requiring only information on particle size and the relative fractions of different components. Optical models that explicitly include particle shape are too complex and computationally expensive to be used in this context, as well as having limited constraint from observations. In many cases, different aerosol components are mixed together to form homogeneous "'grey spheres"', each of which has a single complex refractive index that is often estimated through a simple linear volume-weighting mixing rule (e.g. Ghan and Zaveri, 2007; Bellouin et al., 2013). Core/shell bin schemes have also been developed (e.g. Jacobson, 2001; Matsui et al., 2013), but widespread implementation is yet to take place as they are more computationally expensive than grey spheres, and it is yet to be demonstrated that they necessarily give more accurate results. Bond et al. (2006) discussed the limitations of these two types of scheme,

and highlighted the potential of each to reach unphysical results under certain circumstances. Recently, several studies have produced parametrisations to calculate MAC or E_{Abs} for variable internal mixing of BC with other aerosol components (Liu et al., 2017; Chakrabarty and Heinson, 2018; Wu et al., 2018). These have been constructed using some type of empirical fit to MAC or E_{Abs}, using real-world measurements and/or calculations from complex optical models. However, none of these schemes have been explicitly tested on highly aged biomass burning smoke in ambient conditions.

The southeast Atlantic is an excellent natural laboratory for studying the properties of aged smoke during the southern hemisphere biomass burning season, roughly May – October (Zuidema et al., 2016). At this time of year, the southeast Atlantic region is devoid of notable convective clouds that would contribute to removal of aerosol particles from the lofted smoke layers while they remain in the free troposphere. Combined with the high strength of solar radiation in the tropics, this allows the smoke to reach a very high photochemical age. Zuidema et al. (2018) recently reported high values of MAC measured using ground-based instruments on Ascension Island, where aged smoke had entrained into the boundary layer, with equivalent E_{Abs} of 1.7 – 2.3. In this paper we describe results from the CLARIFY field campaign, which involved airborne measurements of black carbon and optical properties in highly aged biomass burning plumes over the southeast Atlantic (Haywood et al., 2020, in prep.). We quantify the range of values of measured MAC and AAE ~~in this highly aged biomass burning smoke in both the boundary layer and free troposphere, and use single-particle measurements of BC mass and mixing state to assess the suitability of several optical models and parametrisations to simulate aerosol absorption in this environment~~and investigate the absorption closure between microphysical and optical properties of BC for highly-aged biomass burning plumes.

2 Experimental

2.1 CLARIFY measurement campaign

The CLARIFY project took place between 16th August and 7th September 2017. The Facility for Airborne Atmospheric Measurements (FAAM) BAe-146 airborne research aircraft was based out of Ascension Island (7.97°S, 14.40°W). Smoke plumes from the African continent take roughly 4 – 8 days to travel from source to the measurement area (Adebiyi and Zuidema, 2016; Gordon et al., 2018). In total, 28 flights were performed, and the total flight duration over all flights amounted to 100 hours. Fig. 1 shows the aircraft tracks of all flights included in this analysis. All science flights took off and landed on Ascension Island. Full details of the rationale and implementation of the flight campaign are given by Haywood et al. (2020, in prep.).

2.2 Instrumentation

The FAAM aircraft was fitted with a suite of instrumentation for making online measurements of the physical and chemical properties of aerosols, cloud microphysics, remote sensing, and meteorological variables such as temperature, pressure, and relative humidity. Only the ~~instrumention~~ instrumentation directly relevant to the measurements presented in this study are described here. Black carbon number and mass concentrations and single-particle mass and mixing state were measured using

a single-particle soot photometer (SP2). The instrumental setup on the aircraft have been described previously (McMeeking et al., 2010). The SP2 measures the scattering cross-section of particles passing though its laser beam, and particles containing refractory black carbon (rBC) are heated to their ~~incandesence~~ incandescence temperature. The intensity of the incandescent light emission is proportional to the mass of rBC in the particle. The SP2 alignment was checked using nebulised 200 nm and 300 nm polystyrene latex spheres, and these measurements were also used to calibrate the SP2's scattering channel. The instrument response to incandescent rBC was calibrated several times throughout the campaign using nebulised Aquadag, in the manner described by Laborde et al. (2012b). In biomass burning plumes the overall uncertainty of the BC mass concentration is $\pm 17\%$ as a combination of 14% uncertainty due to the uncertainty in the calibration, and 9% variability between instruments (Laborde et al., 2012b). Single-particle BC mass was converted to mass-equivalent BC diameter (D_{BC}) using a BC density (ρ_{BC}) of 1.8 $\mathrm{g\,cm^{-3}}$ (Bond and Bergstrom, 2006). We also used leading-edge only (LEO, Gao et al., 2007; Liu et al., 2015) fits to the SP2's scattering measurement to derive the scattering cross-section for BC particles at a wavelength of 1064 nm, and we use a method similar to that described by Taylor et al. (2015) to quality-assure the LEO data. This method is discussed further in the results section. The BC scattering cross-section data can then be combined with an optical model to provide physical properties of the particle, such as the spherical-equivalent shell/core ratio, or the mass ratio (MR) of non-BC to BC components. These optical calculations are discussed in more detail in Sect. 4.

For BC mass measurements, the SP2 detection limits are driven by a gradual drop-off in detection efficiency for particles with BC content less than around 1 fg (102 nm mass-equivalent core diameter (D_{C}) (Schwarz et al., 2010), and a sharp cut-off at 143 fg (533 nm equivalent D_{C}), where the incandescence detector saturates. For particles that saturate the incandescence detector, we assume the BC content is 143 fg. Particles with BC content less than 1 fg are numerous but contain a negligible fraction of the total BC mass. Particles larger than 143 fg BC are rare, and by examining lognormal fits to the BC mass distribution, we estimate the uncertainty in the BC mass concentration caused by detector saturation is less than 1%. The SP2's upper cut-off diameter in terms of total particle diameter (D_{P}, i.e. the coated diameter for coated particles) is not affected by detector saturation in any practical sense, and is determined by aerodynamic limitations of particles entering the inlet, and is likely to be in the region of 1 µm. The instrument inlets are discussed further below. The SP2 single-particle data were also examined for coincidence at high concentrations, which would cause the instrument to undercount the BC number and mass concentrations. The highest BC number concentrations measured were just below 1000 $\mathrm{cm^{-3}}$, and with this high loading 2% of particle detection windows showed coincident particles. To correct for this small bias, the coincident particles were included in the concentrations of BC mass and number concentrations, but not in the single-particle mixing state analysis, as the leading edge scattering signal can only be measured for the first particle in a measurement window.

Under certain conditions, charring can occur as weakly absorbing particles enter the SP2's laser, causing a false black carbon signal. Sedlacek et al. (2018) showed this can occur for fulvic and humic acids (BrC surrogates), but only when they had been passed through an external heated tube furnace, which we do not use in our experiment. Artificial tar balls formed through anoxic pyrolysis may also show a false rBC signal, but tar balls formed in real fires have been observed to show no detectable incandescence signal in the SP2 (Adler et al., 2019). We therefore do not consider this to be a major concern for our observations.

Non-refractory aerosol composition was measured using a compact time-of-flight aerosol mass spectrometer (AMS), which we used to provide mass concentrations of organic aerosol (OA), as well as the major inorganic species SO_4, NO_3, and NH_4. The AMS detection size range is determined by the transmission of the aerodynamic lens on the instrument's inlet, which has transmission efficiency near 100% over the size range 50 – 1000 nm (Liu et al., 2007). The AMS data are used here to provide some context to the black carbon and optical measurements, as well as to calculate the density of the non-BC components. An in-depth discussion of the aerosol chemical composition and vertical profile is presented by Wu et al. (2020). The AMS was calibrated before and after each flight using nebulised ammonium nitrate, and the relative ionisation efficiencies of NH_4 and SO_4 were also calibrated during the campaign by varying the concentrations of nebulised ammonium nitrate and ammonium sulphate (Allan et al., 2004).

Carbon monoxide (CO) concentrations were measured using a vacuum ultraviolet florescence spectroscopy monitor AL5002. The CO data are used as a measure of the amount of pollution throughout the atmospheric profile. The CO monitor was calibrated and zeroed multiples times per flight at different ~~altitudes~~altitudes, and has an overall ~~accruacy~~ accuracy of $\pm 3\%$.

Aerosol absorption coefficient (B_{Abs}) was measured using three separate photoacoustic spectroscopy (PAS) cells, operating at wavelengths of 405 nm, 514 nm, and 655 nm, as part of the new EXtinction, SCattering and Absorption of Light for AirBorne Aerosol Research (EXSCALABAR) suite of instrumentation (Davies et al., 2019; Szpek et al., 2020, in prep.). The PAS instruments sampled behind an impactor with a cut-point of 1.3 µm aerodynamic diameter to remove coarse-mode particles, and a nafion drier to lower the measurement relative humidity (RH) to below 10% within the PAS detection volume. Davies et al. (2018) describe the PAS instrument and ozone calibrations, which were performed before each flight. For long averaging times, the total uncertainty on the B_{Abs} measurement is 8% (Davies et al., 2019).

We calculate MAC by dividing B_{Abs} by the BC mass concentration measured by the SP2, and the systematic uncertainty in MAC of $\pm$ 19% is calculated by combining the relative uncertainties of B_{Abs} and BC mass concentration in quadrature. We also calculate E_{Abs} by dividing the measured MAC by the values reported for fresh BC by Bond and Bergstrom (2006) of 7.5 ± 1.2 m^2 g^{-1} at a wavelength of 550 nm. The uncertainty in E_{Abs} is then 25%, calculated by combining the uncertainty in our measured MAC with the range of MAC from Bond and Bergstrom (2006). AAE was calculated by comparing the absorption coefficient at different wavelengths. The 8% uncertainty in the absorption coefficient applies almost equally to all channels as it derives from a comparison between ozone calibrations and nebulised nigrosin dye (Davies et al., 2018). The uncertainty in AAE is therefore significantly lower than that of individual single wavelength PAS measurements and is expected to be under 5%.

All aerosol concentration measurements were corrected to standard temperature and pressure of 273.15 K and 1013.25 hPa. The inboard aerosol instruments all sampled from Rosemount inlets, and the instrumental setup and detection ranges mean they all sampled a comparable size range of accumulation mode submicron aerosol ~~.~~(Trembath et al., 2012). The main instruments discussed here have slightly different upper cut-off diameters; 1.3 µm for the PAS, 1 µm for the AMS, and around 1 µm for the SP2. Wu et al. (2020) presents aerosol size distributions measured at ambient humidity using a passive cavity aerosol spectrometer probe (PCASP, Droplet Measurement Technologies, model SSP-200). Examination of these size distributions

determined that the difference between a cut-off of 1.0 and 1.3 μm equated to 1.5% in terms of the total particle volume distribution.

In-cloud data were removed when the liquid water content measured by a wing-mounted cloud droplet probe exceeded 0.01 $\mathrm{g\,m^{-3}}$. To prevent noise at low concentrations affecting our measurements, aerosol data were also removed when the BC mass concentration fell below 0.1 $\mathrm{\mu g\,m^{-3}}$ or the absorption coefficient at any wavelength fell below 5 $\mathrm{Mm^{-1}}$.

3 Results

Figure 2 shows vertical profiles describing the average atmospheric conditions measured during CLARIFY in terms of the level of pollution, meteorological variables, and chemical composition of the aerosol. The marine boundary layer (MBL) was capped by an inversion of several degrees Celsius around 1.5 – 2 km in altitude, though the exact altitude and depth of this inversion varied. The RH in the boundary layer increased from 75 % near the surface to ~~to~~ 80% up towards the top of the boundary layer, where a stratocumulus deck was often present, though excluded from our data. Plumes in the free troposphere were much drier but the RH increased with altitude, from 20% at 2 km to 50% at 5 km, and some plumes reached up to 70 – 80%.

The CO and BC profiles show the altitudes at which the biomass burning smoke reached the area around Ascension Island. There was considerable variability in the regimes that were experienced during the aircraft deployment with the pollution confined either to the MBL or free troposphere, or pollution in both the MBL and free troposphere at any particular time (Wu et al., 2020). However, for the purposes of the analysis presented here, where we focus on aerosol intrinsic properties, we simply present average vertical profiles. The highest smoke concentrations were found between the inversion top and around 4.5 km, and no significant concentrations of smoke were intercepted above 5 km. The variability in the free troposphere CO and BC profiles shows the average of many discrete plumes at variable altitudes. The aged smoke particles were in the accumulation mode size range (Wu et al., 2020). Comparing the BC number concentration to the accumulation mode number concentration measured by ~~a passive cavity aerosol spectrometer probe (PCASP)~~the PCASP, the BC number fraction was 39 $\pm$ 7 %. Using the SP2 alone, comparing to the SP2's scattering measurement (which has a more limited detection range), this fraction was 55 $\pm$ 7 %. The exact numbers are sensitive to the lower detection limits of the various measurements, and may therefore vary from probe to probe. Nevertheless, it is clear that a significant fraction of particles contained BC, but also that a significant fraction contained little to no BC.

Panels (e) – (h) in Fig 2 show the ratios of non-refractory aerosol components measured by the AMS, relative to the BC mass concentration, which give an indication of the composition of BC coatings if the particles are internally mixed, as well as the composition of particles that contain little to no BC. OA dominated the aerosol mass. Although the OA/BC ratio profile was relatively constant throughout the profile compared to ratios of some of the inorganic components to BC, it was larger and more variable in the MBL than the FT. In the free troposphere, the $\mathrm{NO_3/BC}$, $\mathrm{NH_4/BC}$ ratios all increased between 2 – 5 km, as did the OA/BC ratio although to a much lesser extent. This is consistent with a change in the equilibrium of semi-volatile species to favour the condensed phase at lower temperatures, which is discussed in more detail by Wu et al. (2020). However, these

differences may also be related to different ageing and/or sources between the smoke layers measured at different altitudes. The increased sulphate and ammonium in the MBL compared to the free troposphere suggests a marine influence to the aerosol, and the variability of these components in the MBL is due to variation in the relative contributions of biomass burning smoke and marine aerosol.

Figure 3 shows average vertical profiles of BC properties and MAC. The average values of the BC core mass median diameter (MMD) are slightly smaller than most field measurements of biomass burning ~~(e.g. Sahu et al., 2012; Taylor et al., 2014)~~ (e.g. Kondo et al., 2011; Sahu et al., 2012; Taylor et al., 2014), which tend to be in the range 190 – 215 nm, but they are still larger than laboratory burns by May et al. (2014), which were in the range 170 $\pm$ 20 nm. Holder et al. (2016) also reported that the MMD of fresh BC from biomass burning was source dependant, showing that grass such as from savannah sources in southern and central Africa produced smaller BC cores. The count median diameter (CMD) values are also reported here, as they can be a useful indicator of different sources or be an indication of cloud processing. Literature comparisons of CMD are difficult, as the CMD is sensitive to the lower cut-off diameter of the instrument, which varies between instruments (Laborde et al., 2012b). The vertical profiles show no strong trends in CMD and MMD, though both distributions were shifted a few nanometres lower in the boundary layer compared to the free troposphere. This shift could be due to different source regions, or wet removal processes in the boundary layer preferentially removing the largest particles, though to a much lesser extent than described by Taylor et al. (2014).

Figure 3 (c) shows the profile of median BC MR and the spherical-equivalent shell/core ratios, assuming a concentric core/shell geometry of a BC core coated by non-BC material. The average values show significant internal mixing throughout the profile, and compare well to previous measurements of aged biomass burning smoke (e.g. Taylor et al., 2014, and references therein). The equivalent median absolute coating thicknesses were around 90 nm in the boundary layer, similar to aged smoke in Amazonia (Darbyshire et al., 2019), and up to 120 nm in the free troposphere. BC coatings increased with altitude; the median shell/core ratios were around 2.3 in the boundary layer, increasing up to around 2.6 between 4 – 5 km. This trend is likely to be related to the increase with altitude of condensed phase semi-volatiles such as ammonium nitrate in the free troposphere, as shown in Fig. 2.

Figure 3 (d) – (f) show the average vertical profiles of MAC at the three measurement wavelengths, and the campaign average values are also shown as a function of wavelength in Fig. 4. The average values were 20 ± 4 $\mathrm{m^2 g^{-1}}$, 15 ± 3 $\mathrm{m^2 g^{-1}}$, and 12 ± 2 $\mathrm{m^2 g^{-1}}$ at wavelengths of 405 nm, 514 nm, and 655 nm respectively. These values are around a factor of ~~1.8~~ 1.85 $\pm$ 0.45 higher than that expected of fresh, externally mixed BC, reported by Bond and Bergstrom (2006). This high absorption enhancement ($E_{\text{Abs-MAC}}$, the ratio of the measured MAC to the values reported by Bond and Bergstrom (2006)) is conceptually consistent with the high measured coating thicknesses, although the exact modelled values will depend on which optical model is used. The vertical variability in MAC was of the order of a few percent, and was smaller than the uncertainty of $\pm 19\%$ associated with the MAC calculation.

Alongside the mean MAC, Fig. 4 also shows the mean AAE calculated between the three wavelength pairs ($\mathrm{AAE}_{405-514}$, $\mathrm{AAE}_{514-655}$, and $\mathrm{AAE}_{405-655}$ between 405 – 514 nm, 514 – 655 nm, and 405 – 655 nm respectively). The rationale behind examining the different wavelength pairs is that $\mathrm{AAE}_{405-514}$ is most sensitive to BrC absorption at the shorter wavelengths

whereas $AAE_{514-655}$ is less sensitive to BrC, and $AAE_{405-655}$ is most useful for literature comparison. $AAE_{514-655}$ was just below unity, which is within the range expected from absorption by black carbon, with no significant absorption by BrC at these wavelengths. An $AAE_{405-514}$ of around 1.4 suggests a small contribution from BrC to absorption at the shorter wavelengths. There are some uncertainties associated with this approach, in that optical models do not always predict that the AAE of BC is invariant with wavelength. We revisit this calculation in Sect. 4.3, including model estimates of the AAE of BC, and show that to first order this calculation is robust. By extrapolating the BC absorption from the longer wavelengths, we estimate the fractional contribution of BrC to absorption at 405 nm ~~was 10~~ using the equation

$$F_{\text{BrC-405}} = 1 - \frac{\text{MAC}_{514}}{\text{MAC}_{405}} \left(\frac{514}{405}\right)^{\text{AAE}_{514-655}},$$

where $F_{\text{BrC-405}}$ is the fraction of absorption at a wavelength of 405 nm due to BrC, and MAC_{405} and MAC_{514} are the measured MAC at wavelengths of 405 nm and 514 nm respectively.

The average value of $F_{\text{BrC-405}}$ was 11 $\pm$ 2%~~. It~~, and it is likely that ~~this~~ the BrC fraction of absorption will increase at even shorter wavelengths in the UV spectrum, although these are less relevant for climatic absorption due to the shape of the solar spectrum. The uncertainty here is extrapolated only from the relative uncertainties between the different PAS absorption wavelengths (<5% for the AAE values), as the BC mass concentration scales the MAC equally at all wavelengths, and drops out of the calculation. The error bars in Fig. 4 are therefore not representative of the uncertainty in this calculation.

It is useful to calculate the effective MAC of the mixture of BrC and non-absorbing OA components, by dividing the calculated BrC absorption by the measured OA mass concentration, as this allows for comparison between different projects. The equation here is of the form

$$\text{MAC}_{\text{OA}} = \text{MAC}_{405} \times F_{\text{BrC-405}} \times \overline{\left[\frac{\text{BC}}{\text{OA}}\right]},$$

using the campaign average ratio of the BC and OA mass concentrations, which was 0.13.

This calculation yields the effective MAC for OA at 405 nm of ~~0.27~~0.31 $\pm$ ~~0.08~~0.09 $\text{m}^2\,\text{g}^{-1}$. ~~Here the~~ The uncertainty is propagated from the relative uncertainties between the different PAS absorption wavelengths and the uncertainty in the OA mass concentration~~.~~, and again the BC mass concentration drops out of the calculation. The measurement size range of the AMS, SP2 and PAS are all limited to the submicron accumulation mode, so the uncertainty due to a mismatch in measurement range should be small. This value is not the MAC of BrC- it is the effective MAC of the mixture of BrC and nonabsorbing OA components. Literature comparison here is difficult as many studies use different wavelengths and different methods to quantify the OA or BrC mass. Two studies using a similar measurement method and wavelength as described here reported values of 0.5 – 1.5 $\text{m}^2\,\text{g}^{-1}$ (Lack et al., 2012) and 0.53 – 0.6 $\text{m}^2\,\text{g}^{-1}$ (Zhang et al., 2016) for BrC absorption fractions of around 30% at similar blue wavelengths. Our calculated effective OA MAC is significantly lower than these studies, which is consistent with the lower BrC absorption fraction measured for this work.

4 Optical modelling

In the previous section we presented an overview of the vertical profiles and properties of aged smoke over the southeast Atlantic measured during the CLARIFY campaign. In this section, we describe the steps required to simulate MAC from the single-particle measurements of BC mass and scattering cross-section, and compare results from a variety of optical models to the measured properties of the aerosol. The framework is built upon a combination of previous work by Taylor et al. (2015) and Liu et al. (2017), and is made up of two distinct halves. The previous work focused on relating the instrument response of the SP2 to physical properties of the particles. Taylor et al. (2015) detailed how to account for the limited detection range of the instrument, and also explored the sensitivities to assumptions about the BC density and refractive index ($\boldsymbol{m}_{\mathrm{BC}}$). Liu et al. (2017) then compared optical models to extensive sets of lab and field measurements to produce a semi-empirical relationship relating BC particles' optical scattering to size and mixing state, essentially characterising how real particles deviate from the core/shell Mie model. Applying these steps generates a set of physical properties of the BC-containing particles, similar to what may exist within a climate model. For the first half, previous work has determined a well-characterised route to determine the size and mixing state of the BC particles with a degree of accuracy (Liu et al., 2017).

These physical properties are then used to test different optical schemes that could be implemented in such a climate model, given the in situ optical properties observations of MAC and AAE above. Here we have freedom to vary the optical model and underlying assumptions, including parameters such as $\boldsymbol{m}_{\mathrm{BC}}$, as would be possible in a climate model. The optical models and parametrisations tested in this analysis are listed in Table 1, and described in detail in supplementary Sect. S1. We have tested the core/shell Mie model, as well as several homogeneous grey sphere models, which utilize a Mie model with a sphere of one single complex refractive index, calculated using different rules to account for the mixing between BC and non-BC components. The different mixing rules are: (i) volume mixing, where the refractive index is averaged weighted by the volume of each component; (ii) Maxwell-Garnett approximation (Markel, 2016), which considers mixing of small particles of BC dispersed throughout a non-BC host medium; and the Bruggeman mixing rule (Markel, 2016), which computes the refractive index of two components dispersed evenly within a particle. We have also tested several parametrisations of either MAC or E_{Abs} (Liu et al., 2017; Chakrabarty and Heinson, 2018; Wu et al., 2018), which are based on empirical or semi-empirical fits to MAC or E_{Abs} for particles with different mixing states using real and/or modelled particle data.

4.1 Deriving a 2-D size and mixing state distribution

The SP2 measures the per-particle BC mass (M_{BC}) and scattering cross-section over a specified collection angle. In studies of BC mixing state, a lookup table is often used to estimate some metric of internal mixing, such as the coated diameter assuming a spherical core/shell morphology. This process is summarised in Figure 2 of Taylor et al. (2015) and associated discussion. Some recent work has focused on the mass ratio (MR) as an alternative metric, defined here as MR$= M_{\text{non-BC}}/M_{\mathrm{BC}}$ (Liu et al., 2017). The advantage of using MR as a metric is that it does not assume anything about particle morphology. The disadvantage is that explicit optical models do not use MR. Commonly-used Mie models work in terms of diameter (or more specifically, the size parameter $\chi = \pi D/\lambda$, where λ is the wavelength), so some measurement or assumption of the densities of both the core

and coating are needed to convert MR into diameter. The process for generating a 2-D mixing state distribution takes several steps, which are shown as a schematic in supplementary Fig. S2, and detailed here:

1. Perform core/shell Mie scattering calculations at 1064 nm to create a 2-D lookup table of scattering cross-section versus core diameter and coated diameter

2. Correct this Mie table to represent light scattering by real BC particles using the empirical correction described by Liu et al. (2017), by calculating the equivalent MR using the diameters and densities of the core and coating. This empirical correction to the core/shell Mie model accounts for the fact that particles with MR < 3 do not scatter light at 1064 nm exactly as described by the core/shell Mie model

3. Convert the single-particle M_{BC} measured by the SP2 to the spherical-equivalent D_{BC}, giving single-particle data of D_{BC} and scattering cross-section

4. Process single-particle data through the table to ~~give~~ calculate the single-particle spherical-equivalent ~~core and~~ shell diameters, including the Liu et al. (2017) correction

5. Convert the single-particle ~~data to equivalent M_{BC} and MR ,~~ shell/core ratio to MR and bin the data into a 2-D distribution of MR vs M_{BC}

6. Correct this distribution for the limited detection range of the SP2, described in further detail in supplementary Sect. S3

Steps 1 and 2 are purely theoretical calculations, whereas steps 3 – 6 involve processing of the measured data. These steps require knowledge of several intrinsic properties of the particles. A BC density of $\rho_{\mathrm{BC}} = 1.8\ \mathrm{g\,cm^{-3}}$ is generally accepted as the best estimate after the review by Bond and Bergstrom (2006). Previous work has shown that using the Mie core/shell model with this density and a BC refractive index $\boldsymbol{m}_{\mathrm{BC}} = (2.26 - 1.26i)$ produces good agreement for externally mixed BC particles for scattering at 1064 nm (Moteki et al., 2010; Taylor et al., 2015). These values were also used to derive the empirical correction by Liu et al. (2017). For the refractive index of the shell's non-BC components ($\boldsymbol{m}_{Shell}$), we used a value of $1.5 - 0i$ as in previous work (e.g. Schwarz et al., 2008; Taylor et al., 2015; Liu et al., 2017). Using a non-absorbing coating assumes that BrC makes no direct contribution to absorption. The impact of this assumption will be discussed in the next section. The density of non-BC components was calculated by volume mixing using the relative fractions of the AMS composition, applying densities of 1.2 $\mathrm{g\,cm^{-3}}$ for OA, 1.77 $\mathrm{g\,cm^{-3}}$ for inorganic components (Cross et al., 2007), assuming there is no chemical difference between the BC coating and the bulk non-BC mass of the aerosol.

Figure 5 shows ~~a 2D~~ an example 2-D distribution of BC mass and mixing state (MR versus M_{BC}), which was generated by taking the SP2 measurements and applying the semi-empirical Liu-$E_{\mathrm{Abs/Sca}}$ scheme (steps 4 & 5 above). Equivalent distributions were generated for each straight and level run during the campaign, and the broad features were similar across all the distributions showing biomass burning aerosol. The MR distribution was centred around 20 for 1 fg cores, but was around 7 – 8 for BC larger than a few femtograms. Few particles were in the bottom bin, of MR = 0 for externally mixed particles. The distribution has been corrected for the size-dependent detection efficiency of the SP2 instrument (step 6 above), using the

approach described by Taylor et al. (2015), and discussed in more detail in Sect. ~~S2~~S3. Previous studies have used a core/shell Mie model to relate the light scattering properties of particles to their coating properties. The Liu-$E_{\mathrm{Abs/Sca}}$ is an empirical correction to the core/shell Mie model that accounts for the fact that particles with MR < 3 do not scatter light exactly as described by the core/shell Mie model at 1064 nm. In our dataset the vast majority of particles had MR >3, and therefore were in the regime where the Liu-$E_{\mathrm{Abs/Sca}}$ parametrisation shows that light scattering at 1064 nm is well represented by the core/shell Mie model.

Taylor et al. (2015) investigated the effect of uncertainties associated with assumed parameters on the derived coating thicknesses. Here we performed a Monte Carlo analysis to calculate the combined uncertainty in the derived coating properties and MR. A description of the Monte Carlo approach, as well as a summary of the results, is presented in Sect. ~~S3~~S4. While the uncertainties in the shell/core ratios and absolute coating thicknesses were around 6 – 8%, the uncertainty in the average MR was around 20%. This larger uncertainty is likely due to the larger uncertainty in the density of the coating material. In the next section we use the 2-D distributions of MR versus M_{BC} as input for various optical models to generate absorption properties, and discuss the uncertainty associated with these calculations.

4.1.1 ~~MAC and AAE calculations~~

4.2 MAC and AAE calculations

Having established the properties of the measured particles in terms of M_{BC} and MR, it is then possible to use the different optical models in Table 1 to calculate the MAC of the BC particles. The overall process is in some ways conceptually similar to the last section, but starts with the 2-D distribution of MR vs M_{BC}, rather than the single particle data, and outputs the ensemble mean absorption coefficient. The different optical models described in Sect. S1 were used to calculate tables of absorption cross-section on the same grid as the 2-D particle distributions, converting to spherical-equivalent diameters where necessary using the same densities as in the previous section. We used a full 2-D bin scheme as absorption calculations using modal schemes, which assume a particular value of M_{BC} or MR, may show significant deviations from explicit calculations (Fierce et al., 2020). The uncertainties associated with the MAC and AAE calculations from the different optical models were calculated using the Monte Carlo analysis described in Sect. ~~S3~~S4.

For calculating absorption at visible wavelengths, various values of $\boldsymbol{m}_{\mathrm{BC}}$ were tested in the Mie models, and these are listed in Table S1. For the parametrisations we used the values used in their derivation. The rationale behind varying $\boldsymbol{m}_{\mathrm{BC}}$ in this way is simply to explore the sensitivity to this parameter. There is no consensus on the best value of $\boldsymbol{m}_{\mathrm{BC}}$ (or if there is one fixed value), and different studies use different values, often with little explanation as to why a particular value has been chosen. Bulk measurements of visible absorption suggest values in the range specified by Bond and Bergstrom (2006), and these values are also used in some climate models (e.g. Conley et al., 2012). The aim of our study is to investigate the performance of different models within the framework of how they are currently implemented or could be implemented in the future, rather than to use our results to determine the best value of $\boldsymbol{m}_{\mathrm{BC}}$. Since these particles are unlikely to be perfectly spherical, any Mie model of

their optical properties is an approximation, so it is feasible that absorption and scattering could vary from model predictions in different ways at different wavelengths.

For each of the three measurement wavelengths, Figs. 6 and 7 show the average values of MAC and AAE for 71 straight and level runs measured during CLARIFY at altitudes between 50 – 5700 m, calculated using the various aforementioned optical models, alongside the average of the ambient observations. The use of straight and level runs allows us to have longer averaging times (typically 5 – 15 mins), minimising statistical uncertainties, as well as negating any possibly data misalignments due to different length sample lines. The horizontal axes in Fig. 6 are k_{BC}, the imaginary component of $\boldsymbol{m}_{\mathrm{BC}}$, but it is important to recognise that the real part of the refractive index was varied simultaneously according to Table S1. Run-to-run variability in the modelled and measured values was of the order a few percent, so comparing the campaign average values is appropriate here.

Modelled MAC values varied significantly between models as well as different assumed $\boldsymbol{m}_{\mathrm{BC}}$. The grey sphere models (the dashed lines in Figs. 6 and 7) universally produced values of MAC that were higher than the measured values, other than for the smallest values of $\boldsymbol{m}_{\mathrm{BC}}$ at the blue wavelength. At the green and red wavelengths the modelled MAC was around 20% higher than the measurements for the smallest values of $\boldsymbol{m}_{\mathrm{BC}}$, and up to 100% higher for the largest values of $\boldsymbol{m}_{\mathrm{BC}}$. Meanwhile, at the blue wavelength, the grey sphere models overestimated the MAC by 7 – 60% (dependent on mBC), although this overestimation increased to values in the range 18 – 77% once the effect of BrC had been removed from the MAC estimation. The $\mathrm{AAE}_{514-655}$ values from the grey sphere models agreed well with the measurements for the lowest values of $\boldsymbol{m}_{\mathrm{BC}}$, but were too low for the highest values. $\mathrm{AAE}_{405-514}$ was well below unity for all values of $\boldsymbol{m}_{\mathrm{BC}}$ for all the grey sphere models, and the values produced were outside the range expected for BC even in the absence of BrC (i.e. close to one).

The core/shell Mie model (green lines in Figs. 6 and 7) consistently underestimated MAC at the blue wavelength, but was within the uncertainty of the measurements at the green and red wavelengths for most values of $\boldsymbol{m}_{\mathrm{BC}}$. The blue MAC was 16 – 36% lower than the measured values depending on the value of $\boldsymbol{m}_{\mathrm{BC}}$ whereas the green MAC ranged from 21% below to 13% above the measurements, and the red MAC from 16% below to 29% above the measurements. When the calculated BrC absorption was subtracted, the core/shell Mie values for the blue MAC were still up to 29% lower than the measurements. For most values of $\boldsymbol{m}_{\mathrm{BC}}$, the core/shell Mie model calculations were within the experimental ~~experimental~~ uncertainty of the measured MAC at green and red wavelengths.

The wavelength dependence to the relationship between core/shell model MACs and measured values manifests as low values of AAE values, as shown in Fig. 7. The underprediction of MAC at short wavelengths in the core/shell model is explained in supplementary Sect. ~~S4~~S5. In short, the underprediction by core/shell Mie theory arises because the mixing state and morphology of the measured aerosol is different to that assumed in the derivation of Mie theory. In the Mie and core/shell Mie models, the skin depth effect prevents light interacting fully with all the light absorbing BC, as the surface of the sphere absorbs and scatters light and shields the centre, which is then less effective at absorption (Wang et al., 2015). The reality is that the BC is likely a nonspherical aggregate with a high surface-to-volume ratio, and this high surface area relative to the total BC mass allows light to interact fully with the BC component and the skin depth effect is negligible. Therefore, the skin depth effect causes Mie models to under-predict the light absorption properties for the BC aerosols under investigation here.

See Figure 4(d) vs Figure 4(f) in Chakrabarty and Heinson (2018) for the model calculations that demonstrate this interplay between shielding and the fractal surface-to-volume ratio.

To explicitly demonstrate the effect of the skin-depth shielding, we calculated the MAC based on the E_{Abs} from the core/shell Mie model multiplied by the baseline BC MAC from Bond and Bergstrom (2006), and termed this calculation CS-E_{Abs}. E_{Abs} here refers to the ratio of coated MAC to uncoated MAC within the Mie model, rather than $E_{\mathrm{Abs\text{-}MAC}}$ which is the ratio of coated MAC to the Bond and Bergstrom (2006) values. In contrast to the core/shell Mie model results, the use of CS-E_{Abs} gave MAC values that agreed with the measurements within 18% at all wavelengths and $\boldsymbol{m}_{\mathrm{BC}}$, which was within the experimental uncertainties, whether or not the calculated BrC absorption had been subtracted. The MAC from CS-E_{Abs} was dependent on $\boldsymbol{m}_{\mathrm{BC}}$, but the range of $\boldsymbol{m}_{\mathrm{BC}}$ tested in Fig 6 gave only up to 15% variation in MAC, which was much less sensitive than the other Mie models. The AAE values using CS-E_{Abs} were 0.91 – 0.97, with a very weak dependence on $\boldsymbol{m}_{\mathrm{BC}}$. This range agrees well with the aircraft measurements of $\mathrm{AAE}_{514-655}$, but was well below the measurements of $\mathrm{AAE}_{405-514}$, as expected since the effect of BrC is not accounted for in the model.

The parametrisations shown in Fig. 6 (d) – (f) were generally more successful than the pure Mie models, and the Chak-E_{Abs}, Chak-MAC, and Liu-$E_{\mathrm{Abs/Sca}}$ schemes all gave results within the uncertainty range of the measured MAC. The Chak-MAC parametrisation values of MAC agreed within 6% of the measurements at all wavelengths, and Chak-E_{Abs} predicted MAC values 18 – 21% larger than the measured values when the calculated BrC absorption was removed at 405 nm, or 9 – 18% if not. The results from Liu-$E_{\mathrm{Abs/Sca}}$ agreed within 2% at all wavelengths when the calculated BrC absorption was removed, or 9% if not. The MAC calculations using the Wu-E_{Abs} scheme were around 25% below the measurements at all wavelengths, and there was only a small overlap in the uncertainty ranges between the model and measured values. In terms of AAE, the Liu-$E_{\mathrm{Abs/Sca}}$ and Wu-E_{Abs} parametrisations produced values in excellent agreement with the measured $\mathrm{AAE}_{514-655}$, and the Chak-MAC and Chak-E_{Abs} schemes both have AAE fixed at exactly 1, which was also close to the measured value. All parametrisations underestimated $\mathrm{AAE}_{405-514}$ by some margin, which is expected as they are strictly applicable to black carbon aerosols only and do not account for absorption by BrC.

4.3 Model estimations of the BrC absorption fraction at 405 nm

In the calculations shown in Sect. 3 and Fig. 4, we presented an estimate of the fraction of absorption at 405 nm that was due to the presence of BrC, not BC. This estimate relied on the assumption that the AAE of BC was invariant with wavelength within the visible spectrum. Mie models predict that the AAE of BC is highly dependent on the size of the particles (Lack and Cappa, 2010). When considering a polydisperse BC size distribution, much of this variability will average out, however we conducted some additional calculations to test the robustness of our empirical estimate. The MAC of BC at 405 nm was re-calculated by extrapolating the measured MAC at 655 nm, using the AAE provided by the optical models described earlier in this section, with the full 2-D mixing state of the BC-containing particles. These AAE values are shown in Fig. 7. By using only the models' wavelength dependence of absorption, this approach accounts for the over- or under-prediction of the MAC of BC at the longer wavelengths, which would otherwise have a large effect on the calculated BrC absorption fraction. As in Fig. 4, any absorption in excess to this extrapolation is ascribed to BrC. The results of these calculations are shown in

Table 2. The model results were broadly consistent with our empirical calculation in that they showed that the large majority of absorption was due to BC at this short wavelength. The model-to-model variability was large, and similar in size to the calculated BrC absorption fraction.

5 Discussion

5.1 Physical and optical properties of highly aged biomass burning soot

The main focus of this paper has been the measurement of the physical and optical properties of black carbon in heavily aged biomass burning plumes, and a comparison of the ability of different optical schemes to utilise these physical properties to predict the optical properties. One of the key questions in the field of aerosol absorption is the relative importance of black and brown carbon. This is particularly important in biomass burning plumes, where BrC is thought to have a strong effect near source that diminishes with age (Forrister et al., 2015).

Our measurements have shown that the $AAE_{405-655}$ values in smoke plumes over the southeast Atlantic were always close to 1 (with a mean $AAE_{405-655}$ of ~~1.16~~1.13), which was consistent between our airborne measurements in 2017 and ground-based measurements taken on Ascension the previous year over a similar wavelength range (Zuidema et al., 2018). Previous measurements of savannah fires in southern Africa showed AAE values across the whole visible wavelength range of ≈ 1.8 in relatively fresh plumes, but this was reduced to 1.2 in regional haze layers (Kirchstetter et al., 2004). Our measurements are consistent with this picture of aged haze having a reduced BrC contribution compared to freshly emitted aerosol. Other recent studies have also shown AAE close to 1 in African biomass burning smoke that had been aged for several days (Zuidema et al., 2018; Denjean et al., 2019). These optical properties are also in a similar range to measurements by Saturno et al. (2018), who measured smoke from southern Africa once it had reached Amazonia after 10 days transport. Their measurements found average AAE of ≈ 0.9, and a MAC of 12.3 at 637 nm, equivalent to $E_{\text{Abs-MAC}}$ of 1.9. One of the key features of these African smoke plumes is their long lifetime~~, and after~~ . After several days ageing in the tropical sun, ~~the impact of BrC on visible absorption is minor compared to~~ visible absorption by BrC is dwarfed by absorption by BC.

From a modelling perspective, the BC number fraction is important as it has a large impact on the amount of material assumed to be internally mixed with BC. For example, in the modal aerosol scheme described by Bellouin et al. (2013), as smoke ages it moves almost entirely into what they refer to as a "soluble accumulation mode". Consequently, not only do $\sim$100% of particles contain BC, but all non-BC accumulation mode aerosol is internally mixed with that BC, and this has an important impact on optical properties (Matsui et al., 2018). The exact values for the BC number fraction are difficult to determine due to the different detection limits of the different probes, but the values here ($\sim$40% from SP2/PCASP and $\sim$55% from the SP2 alone) are high compared to our previous measurements of 10% from the SP2 alone in boreal smoke plumes (Taylor et al., 2014), but less than measurements in fresh diesel emissions or flaming plumes which reach 100%. It is important to note that in these aged plumes, the majority of particles by number contain little to no BC, and to ensure that this is replicated in any mixing state scheme used in climate models. The fraction of BC-containing particles is variable in different environments and this is important for calculating the optical properties. However, this number is not widely reported in the

literature since it is operationally defined by the measurements and varies from experiment to experiment. We recommend that in future, effort is given to constraining this number in a range of different environments.

The BC particles measured during CLARIFY were universally thickly coated~~.~~, with median MR values in the range 8 – 12. The concept of "coatings", and the use of optical techniques to measure them, is not always appropriate to describe internal mixing of BC with other material. Recent evidence from laboratory studies and multiple field campaigns (Liu et al., 2017; Pei et al., 2018) shows that for low values of MR, internal mixing with non-BC material takes the form of filling in voids between the soot spherules, and the process of encapsulation only begins for higher values of MR, when the voids have already been filled. Liu et al. (2017) determined that the threshold value of MR, above which particles begin to behave optically in a way that resembles the core/shell model (in terms of E_{Abs} and E_{Sca}), is around 3. Our median MR values were in the range ~~8 – 12, which is in the range~~ where Liu et al. (2017) showed that particles behave like core/shell calculations in terms of light scattering at a wavelength of 1064 nm. The concept of BC coatings therefore does seem to be appropriate for particles with values of MR this high, although it does not necessarily mean that the core/shell Mie model is capable of accurately predicting any or all aspects of optical properties at visible wavelengths. These values of MR, and equivalent shell/core ratios, are higher than most measurements of fossil fuel BC (summarised by Pan et al. (2017)), but similar to some previous measurements of aged biomass and solid fuel burning emissions (e.g. Liu et al., 2014; Taylor et al., 2014), as well as aged pollution in several different regions of China (Gong et al., 2016; Xu et al., 2018; Zhao et al., 2020), and they fall short of the shell/core ratios >3 reported in the stratosphere by Ditas et al. (2018).

Xu et al. (2018) provide a useful summary of previous measurements of E_{Abs}, based on the MAC comparison method used here, thermodenuder comparisons, and an aerosol filtration–dissolution method. Measurements towards the green/red end of the visible spectrum (where BrC has minimal absorption) seem to show a dichotomy between environments where coatings on BC cause a considerable lensing effect, and those where either the BC is largely externally mixed, or the limited internal mixing does not cause a significant lensing effect. Ambient measurements with a strong lensing effect (i.e. with long-wavelength E_{Abs} around 1.5 or greater) tend to be from sites measuring high levels of highly aged pollution (days rather than hours), and particularly in highly polluted environments in Asia; Xu et al. (2018) list several examples from literature, as well as primary measurements of their own, and other more recent studies have also found similar values of E_{Abs} in Beijing (Xie et al., 2019a, b). Our measurements show that highly aged biomass burning soot from southern Africa universally falls into this category, as we found E_{Abs} values of around 2 that were invariant with wavelength, indicating that the absorption enhancement is caused by a lensing effect.

One possible alternative to a lensing effect would be that the MAC of BC itself is this high. However, these values of MAC are well in excess of the range of MAC for externally mixed BC reported in literature (Bond and Bergstrom, 2006), so this explanation is not plausible. Another possibility is that the absorption is significantly affected by particles that are essentially dark brown spherical balls that may be closely related to tar balls, so-called "intermediate absorbers" (IA) described by Adler et al. (2019). By comparing untreated and thermodenuded absorption measurements, the authors demonstrated laboratory measurements of IA with an AAE of 2.4 between 401 and 661 nm, and argued that the presence of IA particles explains their field measurements of an apparent E_{Abs} of 3 at 661 nm. Let us consider a theoretical external mixture of coated BC with AAE

of 1, and IA with AAE of 2.4. If, for example, the E_{Abs} of BC at 655 nm was actually 1.5, and the other 25% of red absorption came from IA, this would propagate to 40% of absorption at 405 nm, and the resultant total $\mathrm{AAE}_{405-655}$ would be 1.45. The apparent blue $E_{\text{Abs-MAC}}$ would then be 2.5. This situation is therefore not consistent with our observations, as our measured $E_{\text{Abs-MAC}}$ was 2.1 at 405 nm, and our measured $\mathrm{AAE}_{405-655}$ from Fig. 4 was ~~1.16~~1.13.

It is important to note that all our measurements took place at dry humidities, and our modelling did not include the effects of aerosol water. Haslett et al. (2019) used a core/shell Mie model to calculate that in aged plumes measured over southern West Africa, the condensation of water at relative humidities up to 98% at the top of an aerosol layer could cause the aerosol optical depth to increase by a factor of over 1.8. Experimental studies of absorption at these high humidities are rare, though Brem et al. (2012) observed that absorption of OM generated by wood pyrolysis increased by over a factor of 2 as the RH increased from 32% to 95%, where scattering only increased by a factor of ~1.4. However, there was little change in absorption at humidities below 80%, and both absorption and scattering showed steep rises at RH greater than 90%. In our dataset these humidities were not reached throughout the bulk of the aerosol plume in the atmospheric column, as shown in Fig. 2, but they were sometimes observed in clear-sky conditions near the top of the boundary layer. The effects of high relative humidity on aerosol absorption are poorly constrained, and although we are not able to provide any further constraint from our measurements, we recommend further study on this topic.

5.2 Optical modelling of highly aged biomass burning soot

The Mie models had mixed success in replicating the measured optical properties. The volume mixing scheme produced values that were too high at long wavelengths for all values of $\boldsymbol{m}_{\mathrm{BC}}$. The Bruggeman and Maxwell-Garnett mixing schemes produced results that were almost identical, and only narrowly fell within the uncertainty of the measurements for the lowest $\boldsymbol{m}_{\mathrm{BC}}$ index tested, $1.75 - 0.63i$, and only at 405 nm when the BrC absorption had been subtracted. However, Bond and Bergstrom (2006) demonstrated that using such a low value of $\boldsymbol{m}_{\mathrm{BC}}$ externally-mixed BC produced MAC that was too low. For uncoated BC, the skin-depth shielding effect would also become more significant, manifesting as low values of AAE. To produce agreement for AAE, $\boldsymbol{m}_{\mathrm{BC}}$ would have to be lowered to physically unrealistic values that fall outside the range of previous measurements.

For the core/shell Mie model, there were several values of $\boldsymbol{m}_{\mathrm{BC}}$ that gave MAC at the red and green wavelengths that agreed within the measurement uncertainties, but only the highest values of $\boldsymbol{m}_{\mathrm{BC}}$ generated MAC that fell within the measurement uncertainties at 405 nm, even when the BrC absorption had been subtracted. The wavelength dependence to this level of agreement is primarily due to the stronger skin-depth shielding effect at this shorter wavelength. We explore the sensitivity of MAC to $\boldsymbol{m}_{\mathrm{BC}}$ in an illustrative example in Fig. 8, using a representative BC size distribution and coating thickness. In fact, within our illustrative example there are no values of $\boldsymbol{m}_{\mathrm{BC}}$ that produce MAC at all three wavelengths that agree with our observations when used in the core/shell model. Absorption initially increases with $\boldsymbol{m}_{\mathrm{BC}}$, but skin depth shielding limits the maximum value of MAC to a value lower than the measurements at 405 nm. Figure 8 also shows that while higher values of $\boldsymbol{m}_{\mathrm{BC}}$ give higher values of MAC, up to a point, they also give lower values of AAE. For all values of $\boldsymbol{m}_{\mathrm{BC}}$ that fall in the region of measurements from literature, the AAE from core/shell Mie theory was well below the range of measured values in CLARIFY. One way around this could be to use a wavelength-dependent $\boldsymbol{m}_{\mathrm{BC}}$, tuned to give realistic values of AAE, but this

would still struggle to be able to produce high enough MAC at 405 nm. For particles of these sizes, there are no values of $\boldsymbol{m}_{\mathrm{BC}}$ that can generate agreement with measured MAC and AAE within the framework of the core/shell Mie model.

The semi-empirical parametrisations were generally more successful at replicating both MAC and $\mathrm{AAE}_{514-655}$. These schemes generated $\mathrm{AAE}_{514-655}$ close to 1 as they either have AAE fixed at exactly 1 (Chak-MAC), or they use E_{Abs} multiplied by the MAC from Bond and Bergstrom (2006), which is fixed at exactly 1. As E_{Abs} has no strong wavelength dependence, all parametrisations gave values of AAE close to 1, and the Liu-$E_{\mathrm{Abs/Sca}}$ and Wu-E_{Abs} schemes gave values just below 1, that agreed with the measured values. All schemes generated $\mathrm{AAE}_{405-514}$ well below the measured values, primarily because they do not include the effects of BrC in the calculations. Comparing to literature, they are well within the range typically associated with BC absorption, and outside the range commonly measured for freshly emitted aerosol containing a high level of BrC (e.g. the AAE values of 2.5 measured by Lack and Langridge, 2013).

While we calculated a number for the effective MAC of bulk OA (including BC coatings and particles containing no detectable amount of BC, as a mixture of BrC and nonabsorbing OA), we have stopped short of determining a value for the imaginary component of the OA refractive index. The MAC of OA can be calculated purely from the absorption and concentration measurements, whereas the refractive index determination requires detailed optical modelling. The implication of such modelling would be that every data point in Figs. 6 and 7 would give a different number. These numbers could only be accurately used in conjunction with the exact assumed BC optical properties associated with the relevant data point. This argument was made by Liu et al. (2015), and it is still valid in the context of this study. For some of the models, the BrC absorption would have to be negative to agree with the MAC measurements. We would have no confidence in the reliability of any estimates of the imaginary component of OA refractive index generated in this way using this dataset.

In terms of MAC, all the parametrisations gave values that agreed within the experimental uncertainties of the measurements, other than Wu-E_{Abs}. The best agreement was with the Chak-MAC and Liu-$E_{\mathrm{Abs/Sca}}$ schemes, which came within a few percent of the measurements at all three wavelengths. It is not immediately clear why there is a difference between the Chak-E_{Abs} and Wu-E_{Abs} schemes, as they are conceptually similar in the way they were generated. We speculate that it may either be related to some detail of the morphology of the particles used in their simulations, or some particular details of the optical models or refractive indices used, but it is beyond the scope of this paper to make in-depth comparisons of simulations from literature.

The apparent ~~RI~~ dependence of the E_{Abs} parametrisations in Fig. 6 on refractive index is potentially misleading. The CS-E_{Abs} points show that E_{Abs} is not strongly dependent on $\boldsymbol{m}_{\mathrm{BC}}$, meaning this apparent trend is not strongly related to $\boldsymbol{m}_{\mathrm{BC}}$. For values of $\boldsymbol{m}_{\mathrm{BC}}$ in the same region of the horizontal axis in Fig. 6, the CS-E_{Abs} and Liu-$E_{\mathrm{Abs/Sca}}$ schemes came out with almost identical values of MAC. In this environment, with thick BC coatings and high values of MR, these two schemes are essentially the same.

We urge caution however; in low-MR environments such as fossil fuel emissions close to source, the core/shell model is likely to overestimate E_{Abs} as it assumes all non-BC material takes the form of a coating, whereas evidence shows that for low values of MR this non-BC material is more likely to fill internal voids in the soot structure (Pei et al., 2018), which causes minimal absorption enhancement. The Liu-$E_{\mathrm{Abs/Sca}}$ scheme is an empirical fit to correct for this overestimation of E_{Abs}, and

the work by Chakrabarty and Heinson (2018) also included fits to particles with low MR, so these should give better results than the core/shell model in a low-MR environment.

Given the known inaccuracies in the Mie models when calculating the optical properties of atmospheric soot, and the success of some of the parametrisations in replicating the absorption properties of highly aged biomass burning aerosol, we recommend future work should investigate how to implement these types of schemes in a climate model. However, the parametrisations we have used remain incomplete for this purpose. A significant fraction, sometimes the majority, of visible light scattering in aged biomass burning plumes comes from particles containing black carbon. The scattering enhancement from ~~BC coatings~~ coatings on BC-containing particles is an order of magnitude larger than the absorption enhancement, particularly at high humidities (Wu et al., 2018). Liu et al. (2017) considered E_{Sca} at 1064 nm, but visible scattering for these size particles is more sensitive to shape than at 1064 nm. Wu et al. (2018) performed scattering calculations at 532 nm, but only produced a parametrisation for absorption. The ways in which scattering and absorption deviate from Mie calculations are not necessarily the same, and both should be investigated with equal importance if the end goal is to calculate variables like single scattering albedo for radiative forcing calculations.

6 Conclusions

We have presented a series of measurements of aerosol optical properties in southern African biomass burning smoke taken over the southeast Atlantic Ocean 4 – 8 days after emission, and a detailed investigation of the ability of different optical models to replicate these optical properties. Our dataset and analysis are unique in that they are the first set of measurements using high quality absorption and black carbon instruments, and the most detailed investigation of aerosol optical properties, in this type of environment. Our measurements also describe some of the thickest BC coatings, highest absorption enhancements, and most aged smoke plumes ever studied in ambient conditions. Smoke plumes that remain in the free troposphere over the southeast Atlantic have no deposition process, so they have a long lifetime as well as affecting the climate over a vast area thousands of kilometres wide. The high degree of ageing also represents an important real-world test of absorption calculations, which are normally based either on modelled particles, or observations much closer to source or in the laboratory.

Plumes were intercepted in the boundary layer and free troposphere up to altitudes of around 5 km, and the smoke was relatively ~~homogenous~~ homogeneous in composition and optical properties. Based on measurements of the wavelength dependence of absorption, we estimate that BrC contributed around ~~10~~11 ± 2% of absorption at 405 nm, with an effective OA MAC of ~~0.27~~0.31 ± ~~0.08~~0.09 $\mathrm{m^2\,g^{-1}}$, but there was no BrC absorption at 514 nm and 655 nm. Absorption was dominated by black carbon, and thick coatings caused a wavelength-independent absorption enhancement of a factor of ~~1.8~~ 1.85 ± 0.45 compared to uncoated BC.

Mie models were able to successfully replicate some aspects of BC absorption, but failed at others, and absorption in all models was strongly sensitive to the assumed refractive index of the BC. To agree with the measured MAC and AAE, homogeneous grey sphere models would be required to use an unrealistically low value of the BC refractive index. The core/shell model produced MAC in the right range at the green/red end of the visible spectrum, but was unable to produce high enough values at

blue wavelengths for any value of m_{BC}, and underestimated AAE by a significant margin. Some previous studies have shown that the core/shell model overestimates absorption enhancement for soot particles with lower levels of non-refractory material, where coating is not an accurate description of the mixing state. Instead, our studies on thickly-coated particles demonstrate that the core/shell Mie model underestimates the MAC of the underlying BC at short wavelengths, with this underestimation in MAC caused by the optical skin depth of BC preventing light interaction with the total BC mass in a core/shell model that would otherwise occur in the true agglomerate structure of soot. There is no guarantee that the best implementation of a Mie model for our dataset would be the same for different environments, such as urban measurements closer to source. We recommend any Mie model must be used with caution, if at all, when calculating aerosol absorption.

Two of the four semi-empirical absorption parametrisations we tested produced results that agreed with our observations for MAC within a few percent at all wavelengths, and three within the experimental uncertainties of the field measurements. Two parametrisations produced AAE values in the range of the aircraft measurements at the green/red end of the visible spectrum, but all underestimated AAE in the blue/green range as they did not include the contribution of BrC. Almost all the Mie calculations gave values below the range of measured AAE. This work has been unique in testing the validity of these parametrisations for highly aged, thickly coated particles using real-world observations, and we have shown a good level of success for these schemes. Similar parametrisations should be developed for light scattering by internally mixed BC particles, and together these schemes may then be used to improve estimates of the aerosol direct and semi-direct effects.

Data availability. Airborne measurements are available from the Centre for Environmental Data Analysis https://catalogue.ceda.ac.uk/uuid/38ab7089781a4560b067dd6c20af3769.

Author contributions. JWT prepared the manuscript and performed the bulk of the data analysis, with input from all coauthors. JWT, KB, IC, MF, PIW, JD, JML, MIC, CF, NWD, JMH and HC carried out the airborne measurements. JWT, HW, KS, IC, and JML processed the aircraft data. JML, MIC and HC advised on the data analysis. JMH, JML and HC are lead PIs who led the funding application and directed the research.

Competing interests. The authors declare no competing interests.

Acknowledgements. We thank everyone involved in the planning and execution of the CLARIFY project, as well as our hosts on Ascension Island. The BAe-146-301 Atmospheric Research Aircraft was flown by Airtask and managed by the Facility for Airborne Atmospheric Measurements (FAAM), which is a joint entity of the Natural Environment Research Council (NERC) and the Met Office. CLARIFY was supported by NERC under grants NE/L013584/1 and NE/L013797/1.

References

Adebiyi, A. A. and Zuidema, P.: The role of the southern African easterly jet in modifying the southeast Atlantic aerosol and cloud environments, Quarterly Journal of the Royal Meteorological Society, 142, 1574–1589, https://doi.org/10.1002/qj.2765, http://doi.wiley.com/10.1002/qj.2765, 2016.

Adler, G., Wagner, N. L., Lamb, K. D., Manfred, K. M., Schwarz, J. P., Franchin, A., Middlebrook, A. M., Washenfelder, R. A., Womack, C. C., Yokelson, R. J., and Murphy, D. M.: Evidence in biomass burning smoke for a light-absorbing aerosol with properties intermediate between brown and black carbon, Aerosol Science and Technology, 53, 976–989, https://doi.org/10.1080/02786826.2019.1617832, https://www.tandfonline.com/doi/full/10.1080/02786826.2019.1617832, 2019.

Akagi, S. K., Craven, J. S., Taylor, J. W., McMeeking, G. R., Yokelson, R. J., Burling, I. R., Urbanski, S. P., Wold, C. E., Seinfeld, J. H., Coe, H., Alvarado, M. J., and Weise, D. R.: Evolution of trace gases and particles emitted by a chaparral fire in California, Atmospheric Chemistry and Physics, 12, 1397–1421, https://doi.org/10.5194/acp-12-1397-2012, http://www.atmos-chem-phys.net/12/1397/2012/acp-12-1397-2012.html, 2012.

Allan, J. D., Delia, A. E., Coe, H., Bower, K. N., Alfarra, M., Jimenez, J. L., Middlebrook, A. M., Drewnick, F., Onasch, T. B., Canagaratna, M. R., Jayne, J. T., and Worsnop, D. R.: A generalised method for the extraction of chemically resolved mass spectra from Aerodyne aerosol mass spectrometer data, Journal of Aerosol Science, 35, 909–922, https://doi.org/10.1016/j.jaerosci.2004.02.007, http://dx.doi.org/10.1016/j.jaerosci.2004.02.007, 2004.

Bahreini, R., Ervens, B., Middlebrook, A. M., Warneke, C., de Gouw, J. A., DeCarlo, P. F., Jimenez, J. L., Brock, C. A., Neuman, J. A., Ryerson, T. B., Stark, H., Atlas, E., Brioude, J., Fried, A., Holloway, J. S., Peischl, J., Richter, D., Walega, J., Weibring, P., Wollny, A. G., and Fehsenfeld, F. C.: Organic aerosol formation in urban and industrial plumes near Houston and Dallas, Texas, Journal of Geophysical Research, 114, D00F16, https://doi.org/10.1029/2008JD011493, http://doi.wiley.com/10.1029/2008JD011493, 2009.

Bellouin, N., Mann, G. W., Woodhouse, M. T., Johnson, C., Carslaw, K. S., and Dalvi, M.: Impact of the modal aerosol scheme GLOMAP-mode on aerosol forcing in the Hadley Centre Global Environmental Model, Atmospheric Chemistry and Physics, 13, 3027–3044, https://doi.org/10.5194/acp-13-3027-2013, http://www.atmos-chem-phys.net/13/3027/2013/acp-13-3027-2013.html, 2013.

Bohren, C. F. and Huffman, D. R.: Absorption and scattering of light by small particles, Wiley, New York, 1983.

Bond, T. C. and Bergstrom, R. W.: Light absorption by carbonaceous particles: An investigative review, Aerosol Science and Technology, 40, 27–67, https://doi.org/10.1080/02786820500421521, 2006.

Bond, T. C., Habib, G., and Bergstrom, R. W.: Limitations in the enhancement of visible light absorption due to mixing state, Journal of Geophysical Research, 111, D20 211, https://doi.org/10.1029/2006JD007315, http://doi.wiley.com/10.1029/2006JD007315, 2006.

Bond, T. C., Doherty, S. J., Fahey, D. W., Forster, P. M., Berntsen, T., DeAngelo, B. J., Flanner, M. G., Ghan, S., Kärcher, B., Koch, D., Kinne, S., Kondo, Y., Quinn, P. K., Sarofim, M. C., Schultz, M. G., Schulz, M., Venkataraman, C., Zhang, H., Zhang, S., Bellouin, N., Guttikunda, S. K., Hopke, P. K., Jacobson, M. Z., Kaiser, J. W., Klimont, Z., Lohmann, U., Schwarz, J. P., Shindell, D., Storelvmo, T., Warren, S. G., and Zender, C. S.: Bounding the role of black carbon in the climate system: A scientific assessment, Journal of Geophysical Research: Atmospheres, 118, 1–173, https://doi.org/10.1002/jgrd.50171, http://doi.wiley.com/10.1002/jgrd.50171, 2013.

Brem, B. T., Gonzalez, F. C., Meyers, S. R., Bond, T. C., and Rood, M. J.: Laboratory-measured optical properties of inorganic and organic aerosols at relative humidities up to 95%, Aerosol Science and Technology, 46, 178–190, https://doi.org/10.1080/02786826.2011.617794, http://www.tandfonline.com/doi/abs/10.1080/02786826.2011.617794, 2012.

Browne, E. C., Zhang, X., Franklin, J. P., Ridley, K. J., Kirchstetter, T. W., Wilson, K. R., Cappa, C. D., and Kroll, J. H.: Effect of heterogeneous oxidative aging on light absorption by biomass burning organic aerosol, Aerosol Science and Technology, 53, 663–674, https://doi.org/10.1080/02786826.2019.1599321, https://www.tandfonline.com/doi/full/10.1080/02786826.2019.1599321, 2019.

Canagaratna, M. R., Jayne, J. T., Jimenez, J. L., Allan, J. D., Alfarra, M. R., Zhang, Q., Onasch, T. B., Drewnick, F., Coe, H., Middlebrook, A., Delia, A., Williams, L. R., Trimborn, A. M., Northway, M. J., DeCarlo, P. F., Kolb, C. E., Davidovits, P., and Worsnop, D. R.: Chemical and microphysical characterization of ambient aerosols with the aerodyne aerosol mass spectrometer., Mass spectrometry reviews, 26, 185–222, https://doi.org/10.1002/mas.20115, http://www.ncbi.nlm.nih.gov/pubmed/17230437, 2007.

Cappa, C. D., Onasch, T. B., Massoli, P., Worsnop, D. R., Bates, T. S., Cross, E. S., Davidovits, P., Hakala, J., Hayden, K. L., Jobson, B. T., Kolesar, K. R., Lack, D. A., Lerner, B. M., Li, S.-M., Mellon, D., Nuaaman, I., Olfert, J. S., Petäjä, T., Quinn, P. K., Song, C., Subramanian, R., Williams, E. J., and Zaveri, R. A.: Radiative absorption enhancements due to the mixing state of atmospheric black carbon., Science (New York, N.Y.), 337, 1078–81, https://doi.org/10.1126/science.1223447, http://www.sciencemag.org/content/337/6098/1078.full, 2012.

Chakrabarty, R. K. and Heinson, W. R.: Scaling Laws for Light Absorption Enhancement Due to Nonrefractory Coating of Atmospheric Black Carbon Aerosol, Physical Review Letters, 121, 218 701, https://doi.org/10.1103/PhysRevLett.121.218701, https://link.aps.org/doi/10.1103/PhysRevLett.121.218701, 2018.

Chang, H. and Charalampopoulos, T. T.: Determination of the Wavelength Dependence of Refractive Indices of Flame Soot, Proceedings of the Royal Society A: Mathematical, Physical and Engineering Sciences, 430, 577–591, https://doi.org/10.1098/rspa.1990.0107, http://rspa.royalsocietypublishing.org/cgi/doi/10.1098/rspa.1990.0107, 2006.

Conley, A. J., Garcia, R., Kinnison, D., Lamarque, J.-F., Marsh, D., M., M., Smith, A. K., Tilmes, S., Vitt, F., and Morrison, H.: Description of the NCAR Community Atmosphere Model (CAM 5.0), NCAR Technical Note, NCAR/TN-48, https://doi.org/10.1515/9783111358611-006, 2012.

Cross, E. S., Slowik, J. G., Davidovits, P., Allan, J. D., Worsnop, D. R., Jayne, J. T., Lewis, D. K., Canagaratna, M., and Onasch, T. B.: Laboratory and ambient particle density determinations using light scattering in conjunction with aerosol mass spectrometry, Aerosol Science and Technology, 41, 343–359, https://doi.org/10.1080/02786820701199736, 2007.

Darbyshire, E., Morgan, W. T., Allan, J. D., Liu, D., Flynn, M. J., Dorsey, J. R., O'Shea, S. J., Lowe, D., Szpek, K., Marenco, F., Johnson, B. T., Bauguitte, S., Haywood, J. M., Brito, J. F., Artaxo, P., Longo, K. M., and Coe, H.: The vertical distribution of biomass burning pollution over tropical South America from aircraft in situ measurements during SAMBBA, Atmospheric Chemistry and Physics, 19, 5771–5790, https://doi.org/10.5194/acp-19-5771-2019, https://www.atmos-chem-phys.net/19/5771/2019/, 2019.

Davies, N. W., Cotterell, M. I., Fox, C., Szpek, K., Haywood, J. M., and Langridge, J. M.: On the accuracy of aerosol photoacoustic spectrometer calibrations using absorption by ozone, Atmospheric Measurement Techniques, 11, 2313–2324, https://doi.org/10.5194/amt-11-2313-2018, https://www.atmos-meas-tech.net/11/2313/2018/, 2018.

Davies, N. W., Fox, C., Szpek, K., Cotterell, M. I., Taylor, J. W., Allan, J. D., Williams, P. I., Trembath, J., Haywood, J. M., and Langridge, J. M.: Evaluating biases in filter-based aerosol absorption measurements using photoacoustic spectroscopy, Atmospheric Measurement Techniques, 12, 3417–3434, https://doi.org/10.5194/amt-12-3417-2019, https://www.atmos-meas-tech.net/12/3417/2019/, 2019.

Denjean, C., Bourrianne, T., Burnet, F., Mallet, M., Maury, N., Colomb, A., Dominutti, P., Brito, J., Dupuy, R., Sellegri, K., Schwarzenboeck, A., Flamant, C., and Knippertz, P.: Light absorption properties of aerosols over Southern West Africa, Atmospheric Chemistry and Physics Discussions, pp. 1–40, https://doi.org/10.5194/acp-2019-587, https://doi.org/10.5194/acp-2019-587, 2019.

Ditas, J., Ma, N., Zhang, Y., Assmann, D., Neumaier, M., Riede, H., Karu, E., Williams, J., Scharffe, D., Wang, Q., Saturno, J., Schwarz, J. P., Katich, J. M., McMeeking, G. R., Zahn, A., Hermann, M., Brenninkmeijer, C. A., Andreae, M. O., Pöschl, U., Su, H., and Cheng,

Y.: Strong impact of wildfires on the abundance and aging of black carbon in the lowermost stratosphere, Proceedings of the National Academy of Sciences of the United States of America, 115, E11 595–E11 603, https://doi.org/10.1073/pnas.1806868115, 2018.

Fierce, L., Onasch, T. B., Cappa, C. D., Mazzoleni, C., China, S., Bhandari, J., Davidovits, P., Al Fischer, D., Helgestad, T., Lambe, A. T., Sedlacek, A. J., Smith, G. D., and Wolff, L.: Radiative absorption enhancements by black carbon controlled by particle-to-particle heterogeneity in composition, Proceedings of the National Academy of Sciences of the United States of America, 117, 5196–5203, https://doi.org/10.1073/pnas.1919723117, 2020.

Forrister, H., Liu, J., Scheuer, E., Dibb, J., Ziemba, L., Thornhill, K. L., Anderson, B., Diskin, G., Perring, A. E., Schwarz, J. P., Campuzano-Jost, P., Day, D. A., Palm, B. B., Jimenez, J. L., Nenes, A., and Weber, R. J.: Evolution of brown carbon in wildfire plumes, Geophysical Research Letters, 42, 4623–4630, https://doi.org/10.1002/2015GL063897, http://doi.wiley.com/10.1002/2015GL063897, 2015.

Gao, R. S., Schwarz, J. P., Kelly, K. K., Fahey, D. W., Watts, L. A., Thompson, T. L., Spackman, J. R., Slowik, J. G., Cross, E. S., Han, J.-H. H., Davidovits, P., Onasch, T. B., and Worsnop, D. R.: A Novel Method for Estimating Light-Scattering Properties of Soot Aerosols Using a Modified Single-Particle Soot Photometer, Aerosol Science and Technology, 41, 125–135, https://doi.org/10.1080/02786820601118398, http://dx.doi.org/10.1080/02786820601118398, 2007.

Ghan, S. J. and Zaveri, R. A.: Parameterization of optical properties for hydrated internally mixed aerosol, Journal of Geophysical Research Atmospheres, 112, https://doi.org/10.1029/2006JD007927, http://doi.wiley.com/10.1029/2006JD007927, 2007.

Gong, X., Zhang, C., Chen, H., Nizkorodov, S. A., Chen, J., and Yang, X.: Size distribution and mixing state of black carbon particles during a heavy air pollution episode in Shanghai, Atmospheric Chemistry and Physics, 16, 5399–5411, https://doi.org/10.5194/acp-16-5399-2016, www.atmos-chem-phys.net/16/5399/2016/, 2016.

Gordon, H., Field, P. R., Abe, S. J., Dalvi, M., Grosvenor, D. P., Hill, A. A., Johnson, B. T., Miltenberger, A. K., Yoshioka, M., and Carslaw, K. S.: Large simulated radiative effects of smoke in the south-east Atlantic, Atmospheric Chemistry and Physics, 18, 15 261–15 289, https://doi.org/10.5194/acp-18-15261-2018, https://doi.org/10.5194/acp-18-15261-2018, 2018.

Guyon, P., Boucher, O., Graham, B., Beck, J., Mayol-Bracero, O. L., Roberts, G. C., Maenhaut, W., Artaxo, P., and Andreae, M. O.: Refractive index of aerosol particles over the Amazon tropical forest during LBA-EUSTACH 1999, Journal of Aerosol Science, 34, 883–907, https://doi.org/10.1016/S0021-8502(03)00052-1, 2003.

Haslett, S. L., Taylor, J. W., Deetz, K., Vogel, B., Babic, K., Kalthoff, N., Wieser, A., Dione, C., Lohou, F., Brito, J., Dupuy, R., Schwarzenboeck, A., Zieger, P., and Coe, H.: The radiative impact of out-of-cloud aerosol hygroscopic growth during the summer monsoon in southern West Africa, Atmospheric Chemistry and Physics, 19, 1505–1520, https://doi.org/10.5194/acp-19-1505-2019, https://www.atmos-chem-phys.net/19/1505/2019/, 2019.

Haywood, J. M., Osborne, S. R., Francis, P. N., Keil, A., Formenti, P., Andreae, M. O., and Kaye, P. H.: The mean physical and optical properties of regional haze dominated by biomass burning aerosol measured from the C-130 aircraft during SAFARI 2000, Journal of Geophysical Research: Atmospheres, 108, https://doi.org/10.1029/2002jd002226, http://doi.wiley.com/10.1029/2002JD002226, 2003.

Haywood, J. M., Abel, S. J., Barrett, P., Bellouin, N., Blyth, A., Bower, K. N., Brooks, M., Carslaw, K., Coe, H., Cotterell, M., Crawford, I., Davies, N., Dingley, E., Field, P., Formenti, P., Gordon, H., de Graaf, M., Herbert, R., Johnson, B., Jones, A. C., Langridge, J., Malavelle, F., Partridge, D. G., Peers, F., Redemann, J., Stier, P., Szpek, K., Taylor, J. W., Watson-Parris, D., Wood, R., Wu, H., and Zuidema, P.: Overview of the CLoud-Aerosol-Radiation Interaction and Forcing: Year-2017 (CLARIFY-2017) measurement campaign, Atmospheric Chemistry and Physics, p. in prep, 2020.

Healy, R. M., Wang, J. M., Jeong, C. H., Lee, A. K., Willis, M. D., Jaroudi, E., Zimmerman, N., Hilker, N., Murphy, M., Eckhardt, S., Stohl, A., Abbatt, J. P., Wenger, J. C., and Evans, G. J.: Light-absorbing properties of ambient black carbon and brown carbon from

fossil fuel and biomass burning sources, Journal of Geophysical Research, 120, 6619–6633, https://doi.org/10.1002/2015JD023382, http://doi.wiley.com/10.1002/2015JD023382, 2015.

Hecht, E.: Optics, Pearson Education Limited, Harlow, 4th ed. edn., 2014.

Holder, A. L., Hagler, G. S., Aurell, J., Hays, M. D., and Gullett, B. K.: Particulate matter and black carbon optical properties and emission factors from prescribed fires in the southeastern United States, Journal of Geophysical Research, 121, 3465–3483, https://doi.org/10.1002/2015JD024321, http://doi.wiley.com/10.1002/2015JD024321, 2016.

Jacobson, M. Z.: Strong radiative heating due to the mixing state of black carbon in atmospheric aerosols, Nature, 409, 695–697, 2001.

Kirchstetter, T. W., Novakov, T., and Hobbs, P. V.: Evidence that the spectral dependence of light absorption by aerosols is affected by organic carbon, Journal of Geophysical Research-Atmospheres, 109, 12, https://doi.org/D21208 10.1029/2004jd004999, 2004.

Kondo, Y., Matsui, H., Moteki, N., Sahu, L., Takegawa, N., Kajino, M., Zhao, Y., Cubison, M. J., Jimenez, J. L., Vay, S., Diskin, G. S., Anderson, B., Wisthaler, A., Mikoviny, T., Fuelberg, H. E., Blake, D. R., Huey, G., Weinheimer, A. J., Knapp, D. J., and Brune, W. H.: Emissions of black carbon, organic, and inorganic aerosols from biomass burning in North America and Asia in 2008, Journal of Geophysical Research, 116, D08 204, https://doi.org/10.1029/2010JD015152, http://doi.wiley.com/10.1029/2010JD015152, 2011.

Kroll, J. H., Smith, J. D., Che, D. L., Kessler, S. H., Worsnop, D. R., and Wilson, K. R.: Measurement of fragmentation and functionalization pathways in the heterogeneous oxidation of oxidized organic aerosol., Physical chemistry chemical physics : PCCP, 11, 8005–14, https://doi.org/10.1039/b905289e, http://pubs.rsc.org/en/content/articlehtml/2009/cp/b905289e, 2009.

Laborde, M., Mertes, P., Zieger, P., Dommen, J., Baltensperger, U., and Gysel, M.: Sensitivity of the Single Particle Soot Photometer to different black carbon types, Atmospheric Measurement Techniques, 5, 1031–1043, https://doi.org/10.5194/amt-5-1031-2012, http://www.atmos-meas-tech.net/5/1031/2012/amt-5-1031-2012.html, 2012a.

Laborde, M., Schnaiter, M., Linke, C., Saathoff, H., Naumann, K.-H., Möhler, O., Berlenz, S., Wagner, U., Taylor, J. W., Liu, D., Flynn, M., Allan, J. D., Coe, H., Heimerl, K., Dahlkötter, F., Weinzierl, B., Wollny, A. G., Zanatta, M., Cozic, J., Laj, P., Hitzenberger, R., Schwarz, J. P., and Gysel, M.: Single Particle Soot Photometer intercomparison at the AIDA chamber, Atmospheric Measurement Techniques, 5, 3077–3097, https://doi.org/10.5194/amt-5-3077-2012, http://www.atmos-meas-tech.net/5/3077/2012/amt-5-3077-2012.html, 2012b.

Lack, D. A. and Cappa, C. D.: Impact of brown and clear carbon on light absorption enhancement, single scatter albedo and absorption wavelength dependence of black carbon, Atmospheric Chemistry and Physics, 10, 4207–4220, https://doi.org/10.5194/acp-10-4207-2010, 2010.

Lack, D. A. and Langridge, J. M.: On the attribution of black and brown carbon light absorption using the Ångström exponent, Atmospheric Chemistry and Physics, 13, 10 535–10 543, https://doi.org/10.5194/acp-13-10535-2013, https://www.atmos-chem-phys.net/13/10535/2013/, 2013.

Lack, D. A., Langridge, J. M., Bahreini, R., Cappa, C. D., Middlebrook, A. M., and Schwarz, J. P.: Brown carbon and internal mixing in biomass burning particles., Proceedings of the National Academy of Sciences of the United States of America, 109, 14 802–14 807, https://doi.org/10.1073/pnas.1206575109, http://www.pnas.org/content/109/37/14802.short, 2012.

Lee, H. J., Aiona, P. K., Laskin, A., Laskin, J., and Nizkorodov, S. A.: Effect of solar radiation on the optical properties and molecular composition of laboratory proxies of atmospheric brown carbon, Environmental Science and Technology, 48, 10 217–10 226, https://doi.org/10.1021/es502515r, http://pubs.acs.org/doi/10.1021/es502515r, 2014.

Li, J., Pósfai, M., Hobbs, P. V., and Buseck, P. R.: Individual aerosol particles from biomass burning in southern Africa: 2, Compositions and aging of inorganic particles, Journal of Geophysical Research: Atmospheres, 108, n/a–n/a, https://doi.org/10.1029/2002JD002310, http://dx.doi.org/10.1029/2002JD002310, 2003.

Liu, D., Allan, J. D., Young, D. E., Coe, H., Beddows, D., Fleming, Z. L., Flynn, M. J., Gallagher, M. W., Harrison, R. M., Lee, J., Prevot, A. S. H., Taylor, J. W., Yin, J., Williams, P. I., and Zotter, P.: Size distribution, mixing state and source apportionment of black carbon aerosol in London during wintertime, Atmospheric Chemistry and Physics, 14, 10 061–10 084, https://doi.org/10.5194/acp-14-10061-2014, http://www.atmos-chem-phys.net/14/10061/2014/acp-14-10061-2014.html, 2014.

Liu, D., Taylor, J. W., Young, D. E., Flynn, M. J., Coe, H., and Allan, J. D.: The effect of complex black carbon microphysics on the determination of the optical properties of brown carbon, Geophysical Research Letters, 42, 613–619, https://doi.org/10.1002/2014GL062443, http://doi.wiley.com/10.1002/2014GL062443, 2015.

Liu, D., Whitehead, J., Alfarra, M. R., Reyes-Villegas, E., Spracklen, D. V., Reddington, C. L., Kong, S., Williams, P. I., Ting, Y.-C., Haslett, S., Taylor, J. W., Flynn, M. J., Morgan, W. T., McFiggans, G., Coe, H., and Allan, J. D.: Black-carbon absorption enhancement in the atmosphere determined by particle mixing state, Nature Geoscience, 10, 184–188, https://doi.org/doi:10.1038/ngeo2901, http://dx.doi.org/10.1038/ngeo2901http://10.0.4.14/ngeo2901http://www.nature.com/ngeo/journal/v10/n3/abs/ngeo2901.html{#}supplementary-information, 2017.

Liu, L., Mishchenko, M. I., and Patrick Arnott, W.: A study of radiative properties of fractal soot aggregates using the superposition T-matrix method, Journal of Quantitative Spectroscopy and Radiative Transfer, 109, 2656–2663, https://doi.org/10.1016/j.jqsrt.2008.05.001, https://www.sciencedirect.com/science/article/pii/S002240730800112X, 2008.

Liu, P. S., Deng, R., Smith, K. A., Williams, L. R., Jayne, J. T., Canagaratna, M. R., Moore, K., Onasch, T. B., Worsnop, D. R., and Deshler, T.: Transmission efficiency of an aerodynamic focusing lens system: Comparison of model calculations and laboratory measurements for the aerodyne aerosol mass spectrometer, Aerosol Science and Technology, 41, 721–733, https://doi.org/10.1080/02786820701422278, http://www.tandfonline.com/doi/abs/10.1080/02786820701422278, 2007.

Lund Myhre, C. E. and Nielsen, C. J.: Optical properties in the UV and visible spectral region of organic acids relevant to tropospheric aerosols, Atmospheric Chemistry and Physics, 4, 1759–1769, https://doi.org/10.5194/acp-4-1759-2004, http://www.atmos-chem-phys.net/4/1759/2004/, 2004.

Markel, V. A.: Introduction to the Maxwell Garnett approximation: tutorial, Journal of the Optical Society of America A, 33, 1244, https://doi.org/10.1364/josaa.33.001244, https://www.osapublishing.org/abstract.cfm?URI=josaa-33-7-1244, 2016.

Matsui, H., Koike, M., Kondo, Y., Moteki, N., Fast, J. D., and Zaveri, R. A.: Development and validation of a black carbon mixing state resolved three-dimensional model: Aging processes and radiative impact, Journal of Geophysical Research: Atmospheres, 118, 2304–2326, https://doi.org/10.1029/2012JD018446, http://doi.wiley.com/10.1029/2012JD018446, 2013.

Matsui, H., Hamilton, D. S., and Mahowald, N. M.: Black carbon radiative effects highly sensitive to emitted particle size when resolving mixing-state diversity, Nature Communications, 9, 3446, https://doi.org/10.1038/s41467-018-05635-1, http://www.nature.com/articles/s41467-018-05635-1, 2018.

May, A. A., McMeeking, G. R., Lee, T., Taylor, J. W., Craven, J. S., Burling, I., Sullivan, A. P., Akagi, S., Collett, J. L., Flynn, M., Coe, H., Urbanski, S. P., Seinfeld, J. H., Yokelson, R. J., and Kreidenweis, S. M.: Aerosol emissions from prescribed fires in the United States: A synthesis of laboratory and aircraft measurements, Journal of Geophysical Research: Atmospheres, 119, 11,826–11,849, https://doi.org/10.1002/2014JD021848, http://doi.wiley.com/10.1002/2014JD021848, 2014.

McMeeking, G. R., Hamburger, T., Liu, D., Flynn, M., Morgan, W. T., Northway, M., Highwood, E. J., Krejci, R., Allan, J. D., Minikin, A., and Coe, H.: Black carbon measurements in the boundary layer over western and northern Europe, Atmospheric Chemistry and Physics, 10, 9393–9414, https://doi.org/10.5194/acp-10-9393-2010, http://www.atmos-chem-phys.org/10/9393/2010/acp-10-9393-2010.html, 2010.

Middlebrook, A. M., Bahreini, R., Jimenez, J. L., and Canagaratna, M. R.: Evaluation of Composition-Dependent Collection Efficiencies for the Aerodyne Aerosol Mass Spectrometer using Field Data, Aerosol Science and Technology, 46, 258–271, https://doi.org/10.1080/02786826.2011.620041, http://www.tandfonline.com/doi/abs/10.1080/02786826.2011.620041, 2012.

Mikhailov, E. F., Vlasenko, S. S., Podgorny, I. A., Ramanathan, V., and Corrigan, C. E.: Optical properties of soot-water drop agglomerates: An experimental study, Journal of Geophysical Research-Atmospheres, 111, 16, https://doi.org/D07209 10.1029/2005jd006389, 2006.

Moteki, N., Kondo, Y., and Nakamura, S.: Method to measure refractive indices of small nonspherical particles: Application to black carbon particles, Journal of Aerosol Science, 41, 513–521, https://doi.org/10.1016/j.jaerosci.2010.02.013, 2010.

Pan, X., Kanaya, Y., Taketani, F., Miyakawa, T., Inomata, S., Komazaki, Y., Tanimoto, H., Wang, Z., Uno, I., and Wang, Z.: Emission characteristics of refractory black carbon aerosols from fresh biomass burning: A perspective from laboratory experiments, Atmospheric Chemistry and Physics, 17, 13 001–13 016, https://doi.org/10.5194/acp-17-13001-2017, https://doi.org/10.5194/acp-17-13001-2017, 2017.

Peers, F., Francis, P., Fox, C., Abel, S. J., Szpek, K., Cotterell, M. I., Davies, N. W., Langridge, J. M., Meyer, K. G., Platnick, S. E., and Haywood, J. M.: Observation of absorbing aerosols above clouds over the south-east Atlantic Ocean from the geostationary satellite SEVIRI-Part 1: Method description and sensitivity, Atmospheric Chemistry and Physics, 19, 9595–9611, https://doi.org/10.5194/acp-19-9595-2019, https://www.atmos-chem-phys.net/19/9595/2019/, 2019.

Pei, X., Hallquist, M., Eriksson, A. C., Pagels, J., Donahue, N. M., Mentel, T., Svenningsson, B., Brune, W., and Pathak, R. K.: Morphological transformation of soot: Investigation of microphysical processes during the condensation of sulfuric acid and limonene ozonolysis product vapors, Atmospheric Chemistry and Physics, 18, 9845–9860, https://doi.org/10.5194/acp-18-9845-2018, https://doi.org/10.5194/acp-18-9845-2018, 2018.

Peng, J., Hu, M., Guo, S., Du, Z., Zheng, J., Shang, D., Zamora, M. L., Zeng, L., Shao, M., Wu, Y. S., Zheng, J., Wang, Y., Glen, C. R., Collins, D. R., Molina, M. J., and Zhang, R.: Markedly enhanced absorption and direct radiative forcing of black carbon under polluted urban environments, Proceedings of the National Academy of Sciences of the United States of America, 113, 4266–4271, https://doi.org/10.1073/pnas.1602310113, http://www.ncbi.nlm.nih.gov/pubmed/27035993http://www.pubmedcentral.nih.gov/articlerender.fcgi?artid=PMC4843448, 2016.

Sahu, L. K., Kondo, Y., Moteki, N., Takegawa, N., Zhao, Y., Cubison, M. J., Jimenez, J. L., Vay, S., Diskin, G. S., Wisthaler, A., Mikoviny, T., Huey, L. G., Weinheimer, A. J., and Knapp, D. J.: Emission characteristics of black carbon in anthropogenic and biomass burning plumes over California during ARCTAS-CARB 2008, Journal of Geophysical Research, 117, D16 302, https://doi.org/10.1029/2011JD017401, http://www.agu.org/pubs/crossref/2012/2011JD017401.shtml, 2012.

Saturno, J., Holanda, B. A., Pöhlker, C., Ditas, F., Wang, Q., Moran-Zuloaga, D., Brito, J., Carbone, S., Cheng, Y., Chi, X., Ditas, J., Hoffmann, T., Hrabe De Angelis, I., Könemann, T., Lavrič, J. V., Ma, N., Ming, J., Paulsen, H., Pöhlker, M. L., Rizzo, L. V., Schlag, P., Su, H., Walter, D., Wolff, S., Zhang, Y., Artaxo, P., Pöschl, U., and Andreae, M. O.: Black and brown carbon over central Amazonia: Long-term aerosol measurements at the ATTO site, Atmospheric Chemistry and Physics, 18, 12 817–12 843, https://doi.org/10.5194/acp-18-12817-2018, https://www.atmos-chem-phys.net/18/12817/2018/, 2018.

Sayer, A. M., Hsu, N. C., Eck, T. F., Smirnov, A., and Holben, B. N.: AERONET-based models of smoke-dominated aerosol near source regions and transported over oceans, and implications for satellite retrievals of aerosol optical depth, Atmospheric Chemistry and Physics, 14, 11 493–11 523, https://doi.org/10.5194/acp-14-11493-2014, 2014.

Scarnato, B. V., Vahidinia, S., Richard, D. T., and Kirchstetter, T. W.: Effects of internal mixing and aggregate morphology on optical properties of black carbon using a discrete dipole approximation model, Atmospheric Chemistry and Physics, 13, 5089–5101, https://doi.org/10.5194/acp-13-5089-2013, http://www.atmos-chem-phys.net/13/5089/2013/acp-13-5089-2013.html, 2013.

Schnaiter, M., Linke, C., Mohler, O., Naumann, K.-H., Saathoff, H., Wagner, R., Schurath, U., and Wehner, B.: Absorption amplification of black carbon internally mixed with secondary organic aerosol, Journal of Geophysical Research, 110, D19 204, https://doi.org/10.1029/2005JD006046, http://doi.wiley.com/10.1029/2005JD006046, 2005.

Schwarz, J. P., Spackman, J. R., Fahey, D. W., Gao, R. S., Lohmann, U., Stier, P., Watts, L. A., Thomson, D. S., Lack, D. A., Pfister, L., Mahoney, M. J., Baumgardner, D., Wilson, J. C., and Reeves, J. M.: Coatings and their enhancement of black carbon light absorption in the tropical atmosphere, Journal of Geophysical Research, 113, D03 203, https://doi.org/10.1029/2007JD009042, http://doi.wiley.com/10.1029/2007JD009042, 2008.

Schwarz, J. P., Spackman, J. R., Gao, R. S., Perring, A. E., Cross, E., Onasch, T. B., Ahern, A., Wrobel, W., Davidovits, P., Olfert, J., Dubey, M. K., Mazzoleni, C., and Fahey, D. W.: The Detection Efficiency of the Single Particle Soot Photometer, Aerosol Science and Technology, 44, 612–628, https://doi.org/10.1080/02786826.2010.481298, http://dx.doi.org/10.1080/02786826.2010.481298, 2010.

Sedlacek, A. J., Onasch, T. B., Nichman, L., Lewis, E. R., Davidovits, P., Freedman, A., and Williams, L.: Formation of refractory black carbon by SP2-induced charring of organic aerosol, https://doi.org/10.1080/02786826.2018.1531107, https://www.tandfonline.com/doi/full/10.1080/02786826.2018.1531107, 2018.

Stier, P., Seinfeld, J. H., Kinne, S., and Boucher, O.: Aerosol absorption and radiative forcing, Atmospheric Chemistry and Physics, 7, 5237–5261, 2007.

Szpek, K., Cotterell, M., Davies, N., Fox, C., Tiddeman, D., Wilson, A., Bowles, J., King, R., Kent, J., Smout-Day, R., Richardson, M., Haywood, J., and Langridge, J.: EXSCALABAR - a new instrument for high accuracy measurement of aerosol absorption and extinction from research aircraft, Atmospheric Measurement Techniques, in prep, 2020.

Taylor, J. W., Allan, J. D., Allen, G., Coe, H., Williams, P. I., Flynn, M. J., Le Breton, M., Muller, J. B. A., Percival, C. J., Oram, D., Forster, G., Lee, J. D., Rickard, A. R., Parrington, M., and Palmer, P. I.: Size-dependent wet removal of black carbon in Canadian biomass burning plumes, Atmospheric Chemistry and Physics, 14, 13 755–13 771, https://doi.org/10.5194/acp-14-13755-2014, http://www.atmos-chem-phys.net/14/13755/2014/acp-14-13755-2014.html, 2014.

Taylor, J. W., Allan, J. D., Liu, D., Flynn, M., Weber, R., Zhang, X., Lefer, B. L., Grossberg, N., Flynn, J., and Coe, H.: Assessment of the sensitivity of core / shell parameters derived using the single-particle soot photometer to density and refractive index, Atmospheric Measurement Techniques, 8, 1701–1718, https://doi.org/10.5194/amt-8-1701-2015, http://www.atmos-meas-tech.net/8/1701/2015/, 2015.

Trembath, J., Bart, M., and Brooke, J.: Efficiencies of Modified Rosemount Housings for sampling Aerosol on a Fast Atmospheric Research Aircraft., http://www.faam.ac.uk/index.php/faam-documents/science-instruments/1673-inlet-efficiency, 2012.

Wang, G., Chakrabarti, A., and Sorensen, C. M.: Effect of the imaginary part of the refractive index on light scattering by spheres, Journal of the Optical Society of America A, 32, 1231, https://doi.org/10.1364/josaa.32.001231, https://www.osapublishing.org/abstract.cfm?URI=josaa-32-7-1231, 2015.

Wilcox, E. M.: Stratocumulus cloud thickening beneath layers of absorbing smoke aerosol, Atmospheric Chemistry and Physics, 10, 11 769–11 777, https://doi.org/10.5194/acp-10-11769-2010, http://www.atmos-chem-phys.net/10/11769/2010/, 2010.

Wu, H., Taylor, J. W., Szpek, K., Williams, P. I., Flynn, M., and Others: Vertical variability of the properties of highly aged biomass burning aerosol transported over the southeast Atlantic during CLARIFY-2017, Atmos. Chem. Phys Discuss., https://doi.org/10.5194/acp-2020-197, 2020.

Wu, Y., Cheng, T., Liu, D., Allan, J. D., Zheng, L., and Chen, H.: Light Absorption Enhancement of Black Carbon Aerosol Constrained by Particle Morphology, Environmental Science and Technology, 52, 6912–6919, https://doi.org/10.1021/acs.est.8b00636, http://pubs.acs.org/doi/10.1021/acs.est.8b00636, 2018.

Xie, C., Xu, W., Wang, J., Liu, D., Ge, X., Zhang, Q., Wang, Q., Du, W., Zhao, J., Zhou, W., Li, J., Fu, P., Wang, Z., Worsnop, D., and Sun, Y.: Light absorption enhancement of black carbon in urban Beijing in summer, Atmospheric Environment, 213, 499–504, https://doi.org/10.1016/j.atmosenv.2019.06.041, https://www.sciencedirect.com/science/article/pii/S1352231019304327?via{%}3Dihub, 2019a.

Xie, C., Xu, W., Wang, J., Wang, Q., Liu, D., Tang, G., Chen, P., Du, W., Zhao, J., Zhang, Y., Zhou, W., Han, T., Bian, Q., Li, J., Fu, P., Wang, Z., Ge, X., Allan, J., Coe, H., and Sun, Y.: Vertical characterization of aerosol optical properties and brown carbon in winter in urban Beijing, China, Atmospheric Chemistry and Physics, 19, 165–179, https://doi.org/10.5194/acp-19-165-2019, https://www.atmos-chem-phys.net/19/165/2019/, 2019b.

Xu, X., Zhao, W., Qian, X., Wang, S., Fang, B., Zhang, Q., Zhang, W., Venables, D. S., Chen, W., Huang, Y., Deng, X., Wu, B., Lin, X., Zhao, S., and Tong, Y.: The influence of photochemical aging on light absorption of atmospheric black carbon and aerosol single-scattering albedo, Atmospheric Chemistry and Physics, 18, 16 829–16 844, https://doi.org/10.5194/acp-18-16829-2018, https://www.atmos-chem-phys.net/18/16829/2018/, 2018.

Zhang, J. and Zuidema, P.: The diurnal cycle of the smoky marine boundary layer observed during August in the remote southeast Atlantic, Atmospheric Chemistry and Physics, 19, 14 493–14 516, https://doi.org/10.5194/acp-19-14493-2019, https://www.atmos-chem-phys.net/19/14493/2019/, 2019.

Zhang, X., Kim, H., Parworth, C. L., Young, D. E., Zhang, Q., Metcalf, A. R., and Cappa, C. D.: Optical Properties of Wintertime Aerosols from Residential Wood Burning in Fresno, CA: Results from DISCOVER-AQ 2013, Environmental Science and Technology, 50, 1681–1690, https://doi.org/10.1021/acs.est.5b04134, 2016.

Zhao, D., Liu, D., Yu, C., Tian, P., Hu, D., Zhou, W., Ding, S., Hu, K., Sun, Z., Huang, M., Huang, Y., Yang, Y., Wang, F., Sheng, J., Liu, Q., Kong, S., Li, X., He, H., and Ding, D.: Vertical evolution of black carbon characteristics and heating rate during a haze event in Beijing winter, Science of the Total Environment, 709, https://doi.org/10.1016/j.scitotenv.2019.136251, 2020.

Zhou, X., Ackerman, A. S., Fridlind, A. M., Wood, R., and Kollias, P.: Impacts of solar-absorbing aerosol layers on the transition of stratocumulus to trade cumulus clouds, Atmospheric Chemistry and Physics, 17, 12 725–12 742, https://doi.org/10.5194/acp-17-12725-2017, https://doi.org/10.5194/acp-17-12725-2017, 2017.

Zuidema, P., Redemann, J., Haywood, J., Wood, R., Piketh, S., Hipondoka, M., and Formenti, P.: Smoke and clouds above the southeast Atlantic: Upcoming field campaigns probe absorbing aerosol's impact on climate, https://doi.org/10.1175/BAMS-D-15-00082.1, http://journals.ametsoc.org/doi/10.1175/BAMS-D-15-00082.1, 2016.

Zuidema, P., Sedlacek, A. J., Flynn, C., Springston, S., Delgadillo, R., Zhang, J., Aiken, A. C., Koontz, A., and Muradyan, P.: The Ascension Island Boundary Layer in the Remote Southeast Atlantic is Often Smoky, Geophysical Research Letters, 45, 4456–4465, https://doi.org/10.1002/2017GL076926, http://doi.wiley.com/10.1002/2017GL076926, 2018.

Table 1. List of the different optical models used in this analysis. The absorption calculation column refers to whether the models/parametrisations calculate MAC or E_{Abs}. For those that only calculate E_{Abs}, MAC is calculated by multiplying E_{Abs} by the fresh MAC value from (Bond and Bergstrom, 2006).

	Absorption calculation	Reference
Coated sphere		
Mie core/shell	MAC	(Taylor et al., 2015)
CS-E_{Abs}	E_{Abs}	This study
Homogeneous grey sphere models		
Bruggeman	MAC	(Markel, 2016)
Maxwell-Garnett	MAC	(Bohren and Huffman, 1983)
Volume mixing	MAC	(Bohren and Huffman, 1983)
Semi-empirical parametrisations		
Chak-E_{Abs}	E_{Abs}	(Chakrabarty and Heinson, 2018)
Chak-MAC	MAC	(Chakrabarty and Heinson, 2018)
Liu-$E_{\text{Abs/Sca}}$	E_{Abs}	(Liu et al., 2017)
Wu-E_{Abs}	E_{Abs}	(Wu et al., 2018)

Table 2. BrC absorption fraction at 405 nm (expressed as a percentage) calculated empirically or using the AAE from optical models. The minimum, mean, and maximum refer to the range of results from using the different values of m_{BC}.

	Minimum	Mean	Maximum
Observations			
CLARIFY empirical	-	11 ± 2	-
Optical models			
Core/shell	23	26	33
Bruggeman	13	15	21
Maxwell-Garnett	13	15	20
Volume mixing	13	16	23
Chak-MAC	-	6	-

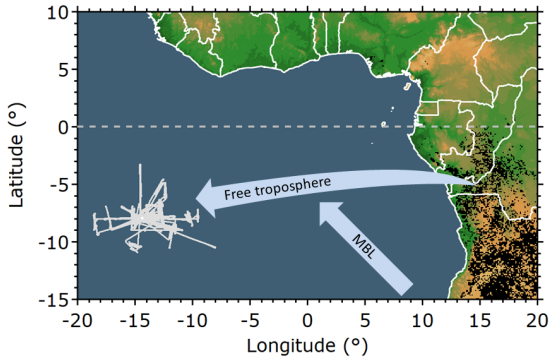

Figure 1. Map showing the location of the CLARIFY aircraft measurements included in this analysis (solid grey trace). The arrows show the approximate mean flow direction in the free troposphere and marine boundary layer (MBL), and the black markers show MODIS fire counts for August – September 2017.

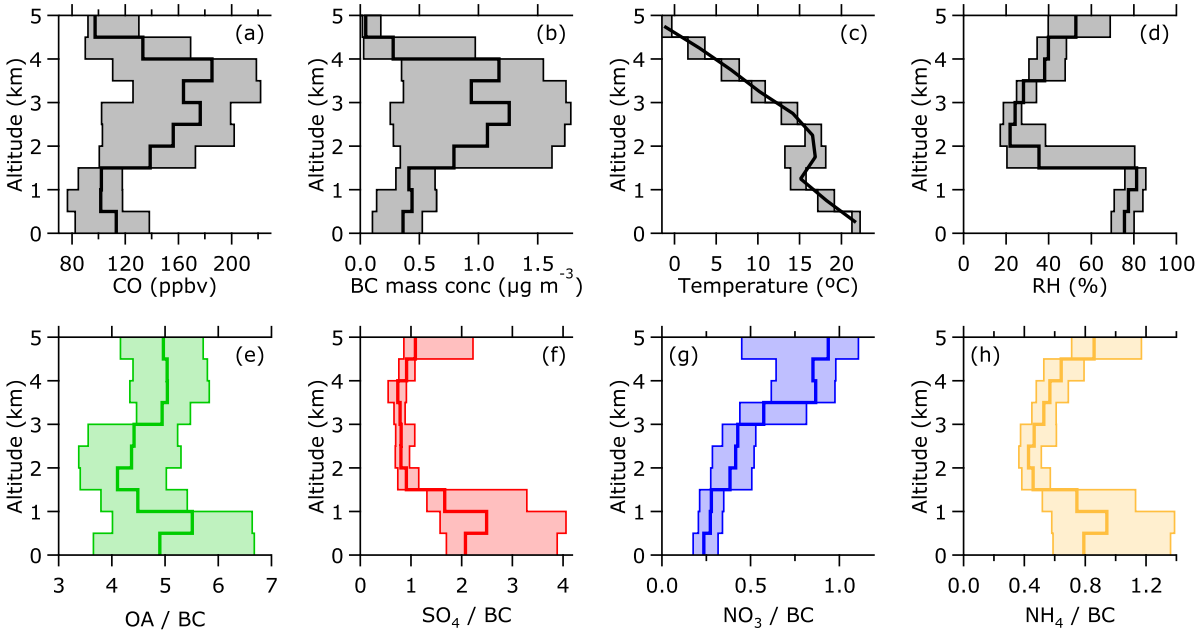

Figure 2. Campaign average vertical profiles of pollution levels, thermodynamic variables, and aerosol chemical composition. The solid lines show the median and the shaded areas show the 25th and 75th percentiles. Panels (c) – (h) show the in-plume data only. Panels (e) – (h) show the ratios of the mass concentrations of organic aerosol and the major inorganic ions to the mass concentration of BC.

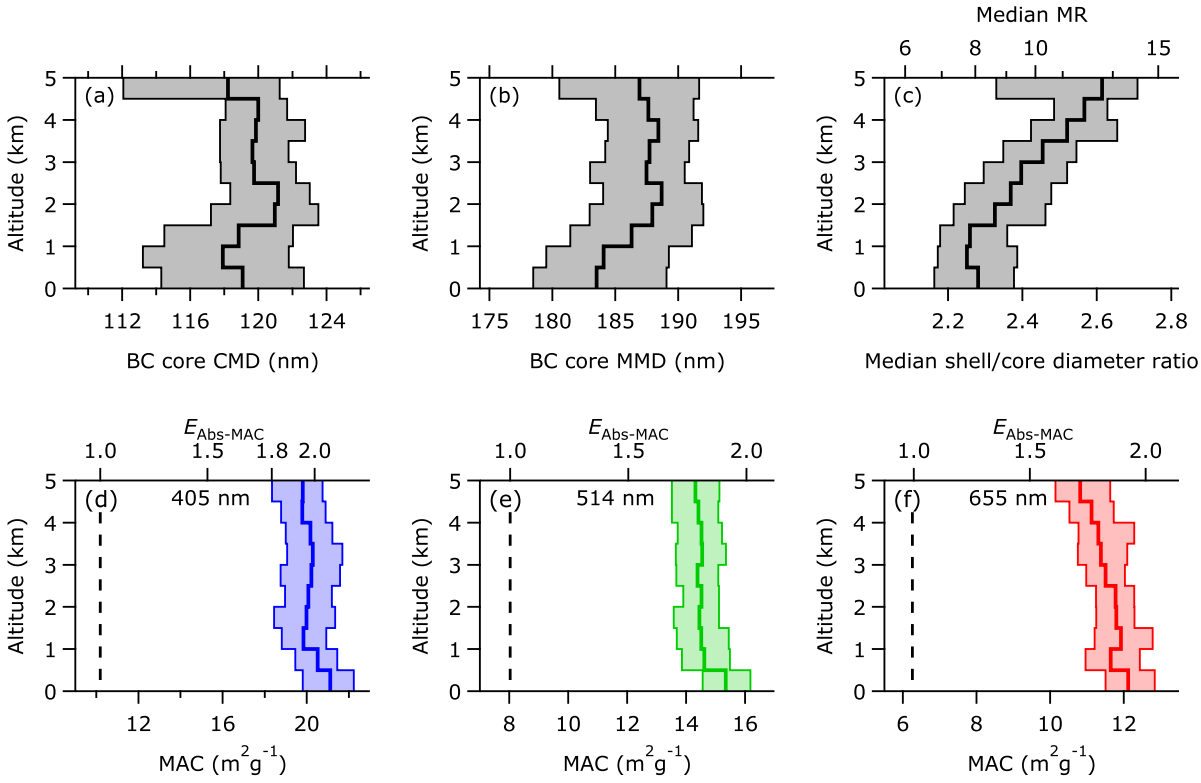

Figure 3. Campaign average vertical profiles of BC properties and MAC. The solid lines show the median and the shaded areas show the 25th and 75th percentiles. Panels (~~b~~a) and (~~e~~b) show the count median diameter and mass median diameter of BC core size distributions, and panel (c) shows the vertical profile of the SP2 shell/core ratio. The E_{Abs} scale in panels (d) – (f) are calculated by dividing the measured MAC by the MAC for uncoated BC reported by Bond and Bergstrom (2006), which is represented by the vertical dashed lines. The uncertainties in the average values are ±19% for MAC and ±25% for E_{Abs}.

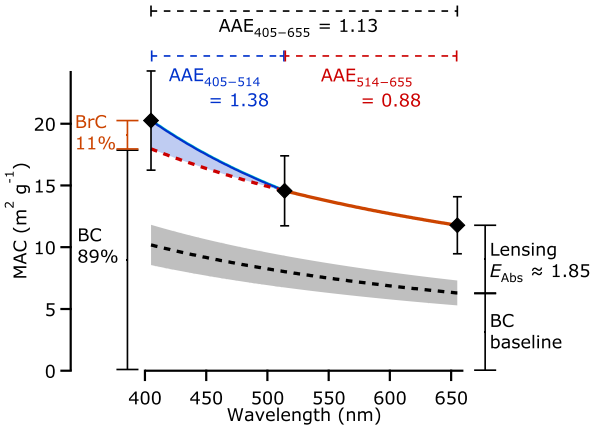

Figure 4. Average measured MAC as at different wavelengths, showing the calculation of the BrC absorption fraction at 405 nm. The black markers are the average CLARIFY measurements, the dashed black line is the BC absorption reported by Bond and Bergstrom (2006), the coloured solid lines represent the wavelength-dependent MAC based on the measured AAE between the two wavelength pairs, while the dashed red line represents the predicted MAC if the measured AAE from the 514 – 655 nm wavelength pair is extrapolated to shorter visible wavelengths.

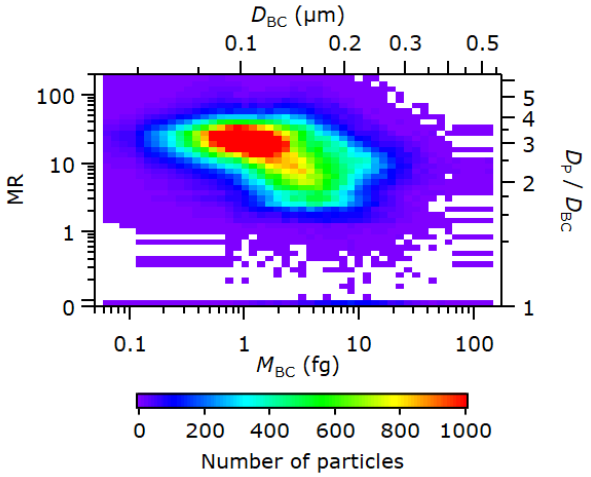

Figure 5. Example 2-D distribution of BC mass and mixing state, corrected for the size-dependent detection efficiency of the instrument (see Sect. ~~S2~~S3). This distribution was taken from one straight and level run on 4 September 2017. The data shown are in terms of M_{BC} and MR on the bottom and left axes, and equivalent values of D_{BC} and shell/core ratio are shown on the top and right axis, assuming $\rho_{BC} = 1.8\ \mathrm{g\,cm^{-3}}$ and $\rho_{Shell} = 1.34\ \mathrm{g\,cm^{-3}}$.

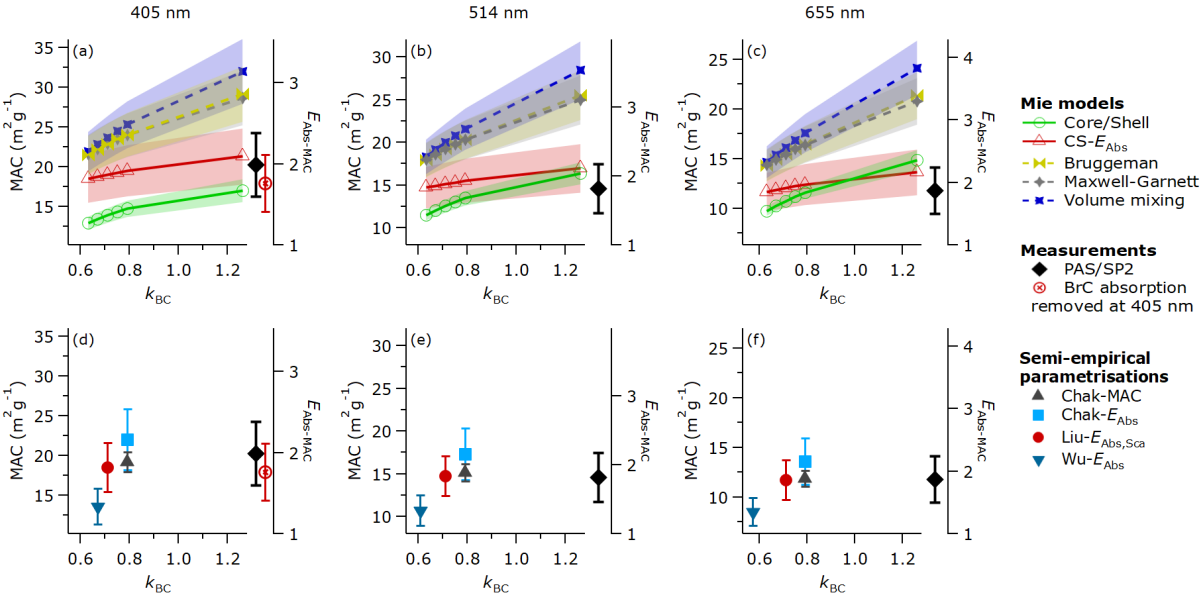

Figure 6. Comparison of measured MAC with values calculated using different optical models at three visible wavelengths. Panels (a) – (c) show different Mie models evaluated at various values of m_{BC}, ~~whereas panels~~ plotted against k_{BC} on the horizontal axis. Panels (d) – (f) show parametrisations which are plotted at the values of k_{BC} at which the parametrisations were developed. The right-hand axes show the equivalent values of E_{Abs} by comparing values to the fresh MAC reported by Bond and Bergstrom (2006). The measured data, displayed as black diamonds to the right of each x-axis, show the weighted mean from the various straight and level runs during CLARIFY, and the errors bars are the systematic uncertainty of 19%. The red markers at 405 nm show the calculated BC MAC with no BrC, extrapolated from the longer wavelengths (see text for further details). The model and parametrisation data show the mean (unweighted) and error bars that are taken from the Monte Carlo analysis described in Sect. ~~S3~~S4, as well as the uncertainty in the fresh MAC reported by Bond and Bergstrom (2006) for the E_{Abs} parametrisations.

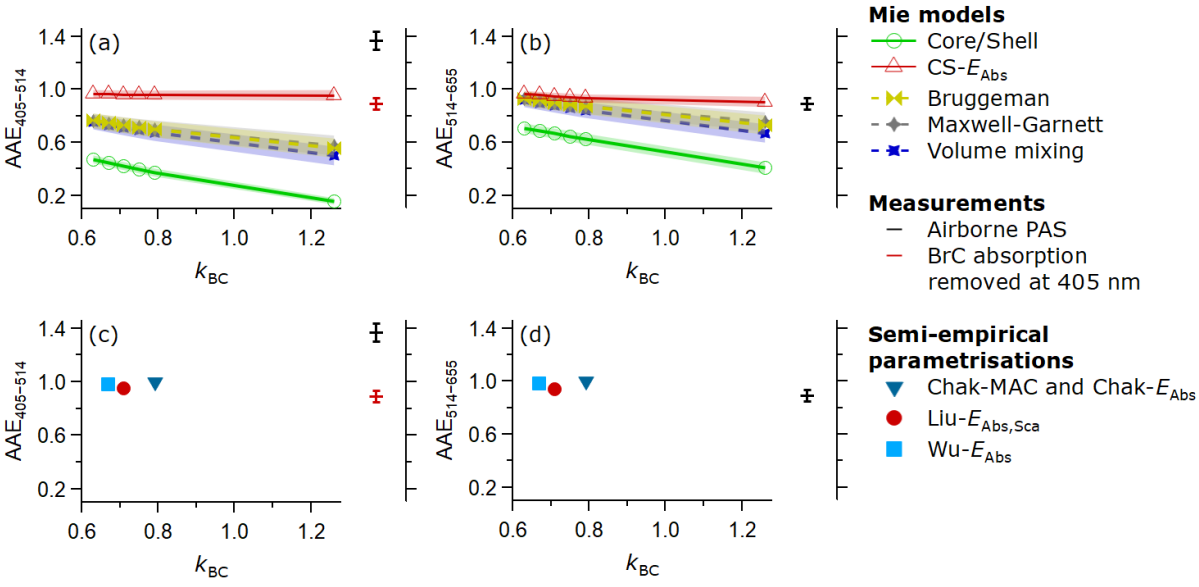

Figure 7. Similar to Fig. 6, but showing AAE from different optical models/parametrisations compared to CLARIFY measurements. Panels (a) and (c) show the AAE between the 405/514 nm wavelength pair, and panels (b) and (d) shows AAE between the 514/655 nm wavelength pair. The error bars are the Monte Carlo errors described in Sect. ~~S3~~S4, and are plotted for all data points, though they are too small to see in some cases. Both schemes by Chakrabarty and Heinson (2018) have fixed AAE of exactly one, so they are listed/plotted together, and have no error bars.

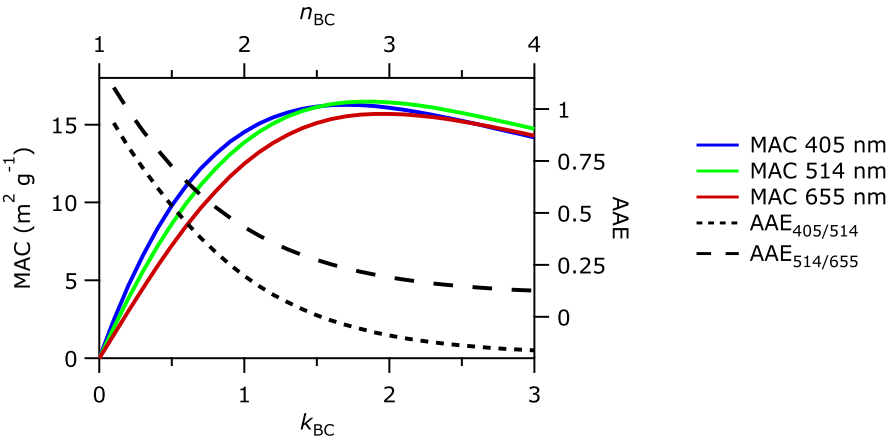

Figure 8. MAC and AAE as a function of $\boldsymbol{m}_{BC}$ for typical core/shell particles measured during CLARIFY. The D_C distribution was taken from Fig. S3a, and representative shell/core ratios of 2.4 were used. Example $\boldsymbol{m}_{BC}$ values follow the rule of $n_{BC} = k_{BC} + 1$, where n_{BC} and k_{BC} are the real and imaginary components of $\boldsymbol{m}_{BC}$. A value of 1.5 - 0i was also used for the shell refractive index.

S1 Optical models and parametrisations

The following sections give descriptions of the various optical models used in this analysis. Only the Liu-$E_{\mathrm{Abs/Sca}}$ parametrisation is used to convert from the single-particle light scattering and M_{BC} measured by the SP2 into MR. This process is described in Sect. 4.1, and this set of calculations is performed using a value of $\boldsymbol{m}_{\mathrm{BC}}$ = (2.26 - 1.26i) at the SP2 instrument wavelength of 1064 nm. All the models are then used to convert the 2D distributions of MR vs M_{BC} into bulk absorption at visible wavelengths, using the range of $\boldsymbol{m}_{\mathrm{BC}}$ listed in Table S1.

Table S1. List of the different values of $\boldsymbol{m}_{\mathrm{BC}}$ used in this study

$\boldsymbol{m}_{\mathrm{BC}}$	Reference
(1.75 - 0.63i)	(Bond and Bergstrom, 2006)
(1.80 - 0.67i)	(Bond and Bergstrom, 2006)
(1.85 - 0.71i)	(Bond and Bergstrom, 2006)
(1.90 - 0.75i)	(Bond and Bergstrom, 2006)
(1.95 - 0.79i)	(Bond and Bergstrom, 2006)
(2.26 - 1.26i)	(Moteki et al., 2010)

S1.1 Coated sphere

The core/shell Mie model considers internally mixed soot particles as consisting of a BC core coated in a non-BC shell, in a morphology of two concentric spheres. It has been implemented in some climate models to calculate bulk scattering and absorption (e.g. Matsui et al., 2013). For calculating absorption, we use two implementations of the core/shell Mie model. For the first we use the core/shell Mie model in its standard form to calculate absorption, and divide by mass to get $\mathrm{MAC_{CS}}$, the MAC calculated using the core/shell Mie model. We also use an additional implementation, termed CS-E_{Abs} where the core/shell model is used to calculate E_{Abs} only, and this is then multiplied by the MAC of uncoated BC to give the coated MAC. The best estimate is provided by Bond and Bergstrom (2006), who summarised previous literature and reported an average value of 7.5 $\mathrm{m^2\,g^{-1}}$ at 550 nm (with AAE = 1), which we refer to as $\mathrm{MAC_{BB}}$. The MAC of internally-mixed BC is then calculated by multiplying E_{Abs} by $\mathrm{MAC_{BB}}$.

S1.2 Homogeneous grey sphere models

We use the term "'grey sphere"' to refer to any model that approximates particles as a homogeneous sphere with a single effective refractive index ($\boldsymbol{m}_{\mathrm{Eff}}$). This approach was described by Stier et al. (2007) and is still used in some climate models (e.g. Bellouin et al., 2013) as it is less computationally expensive than more complex schemes, and requires less constraint. Several mixing rules are possible to calculate the effective refractive index by combining the different components.

Volume mixing

Here the weighted mean refractive index is calculated, with weights determined by the volume fraction of each component

$$\boldsymbol{m}_{\text{Eff}} = \sum_{i=1}^{\infty}(F_i \boldsymbol{m}_i)$$

where F_i and $\boldsymbol{m}_i$ are the volume fraction and refractive index for component i.

The components we considered are BC, OA, ammonium nitrate, and ammonium sulphate, although the non-BC components are all assumed to have the same refractive index.

Bruggeman mixing rule

The Bruggeman mixing rule computes the effective electric permittivity ($\epsilon_{\text{Eff}} = \boldsymbol{m}_{\text{Eff}}^2$) of two components distributed symmetrically. The two components are BC and non-BC, which is a sum of OA, ammonium nitrate, and ammonium sulfate. The permittivity of the non-BC components was calculated using volume mixing. ϵ_{Eff} is then calculated using

$$\epsilon_{\text{Eff}} = \frac{b + \sqrt{8\epsilon_{\text{BC}}\epsilon_{\text{non-BC}} + b^2}}{4}, b = (2F_{\text{BC}} - F_{\text{non-BC}})\epsilon_{\text{BC}} + (2F_{\text{BC}} - F_{\text{non-BC}})\epsilon_{\text{non-BC}},$$

where ϵ_{BC} and $\epsilon_{\text{non-BC}}$ are the electric permittivities and F_{BC} and $F_{\text{non-BC}}$ are the volume fractions of the two components (Markel, 2016, eq. (30)).

Maxwell-Garnett mixing rule

The Maxwell-Garnett mixing rule considers small particles of one component (BC) dispersed evenly in a host medium (non-BC). The non-BC components were summed together as in the Bruggeman mixing rule, and ϵ_{Eff} is calculated using

$$\epsilon_{\text{Eff}} = \left[1 + 3F_{\text{BC}}\left(\frac{\epsilon_{\text{BC}} - \epsilon_{\text{non-BC}}}{\epsilon_{\text{BC}} + 2\epsilon_{\text{non-BC}}}\right) / \left(1 - F_{\text{BC}}\left(\frac{\epsilon_{\text{BC}} - \epsilon_{\text{non-BC}}}{\epsilon_{\text{BC}} + 2\epsilon_{\text{non-BC}}}\right)\right)\right]$$

as given by (Bohren and Huffman, 1983, eq. (8.50)).

S1.3 parametrisations

The Liu-$E_{\text{Abs/Sca}}$ parametrisation

Liu et al. (2017) use an approach that applies an empirical correction to the core/shell Mie model. They compared SP2 measurements of E_{Sca}, the scattering enhancement due to coatings, to $E_{\text{Sca,CS}}$, the equivalent scattering enhancement at 1064 nm for a particle with the same mass and composition but in a concentric core/shell morphology. Liu et al. (2017) based empirical fits to ambient measurements from several locations around the world, and a laboratory study using both fresh and aged diesel soot. Particles of known mass were selected by a centrifugal particle mass analyser (CPMA), and measurements were made of single-particle scattering, as well as bulk properties such as MAC. E_{Abs} and E_{Sca} were also determined by comparing measurements of untreated particles to those passed through a catalytic stripper heated to 400°C designed to remove any non-BC material. Liu et al. (2017) then designed a parametrisation based on an empirical correction to the core/shell Mie model using an internally mixed fraction parameter (F_{in}), which is colloquially known as the 'core/shell-ness'. For low values of MR, BC and non-BC behave optically like externally-mixed spheres. For high values of MR, the particles behave as core/shell particles,

and there exists a transition zone for particles partway between these two regimes. Liu et al. (2017) then define E_{Abs} and E_{Sca} as

$$E_{\text{Abs}} = E_{\text{Abs,CS}} \times F_{\text{in}} + (1 - F_{\text{in}}) \times 1,$$

$$E_{\text{Sca}} = E_{\text{Sca,CS}} \times F_{\text{in}} + (1 - F_{\text{in}}) \times 1,$$

$$\text{where } F_{\text{in}} = \begin{cases} 0, & \text{if MR} < 1.5 \\ 0.57 \times \text{MR} - 0.74, & \text{if } 1.5 \leq \text{MR} < 3 \\ 1, & \text{if MR} \geq 3. \end{cases}$$

It is implicitly assumed that E_{Abs} and E_{Sca} behave in a similar manner using the same values of F_{in}, but the parametrisation is based on measurements of E_{Sca} at $1064\ \text{nm}$. To calculate the coated MAC, we multiplied the calculated E_{Abs} by MAC_{BB}.

The Wu-E_{Abs} parametrisation

Wu et al. (2018) made an empirical fit to the bulk E_{Abs} of simulated BC particles of different mixing states. In their simulation, bare BC particles were generated by diffusion limited aggregation, where BC monomers stick together to form fractal aggregates. Coating material was then added to the surface of these aggregates, in a manner intended to simulate condensation of secondary material onto the soot, as well as coagulation with pre-existing liquid particles resulting in partial encapsulation, and complete encapsulation for higher values of MR. The optical properties of these particles were then calculated using the superposition T-matrix method, averaged for different orientations of the particles, and using a wavelength-dependent $\boldsymbol{m}_{\text{BC}}$ (Chang and Charalampopoulos, 2006). Their empirical fit for E_{Abs} took the form

$$E_{\text{Abs}} = 0.92 + 0.11\, e^{(E_{\text{Abs,CS}} - 1.07)/0.55}.$$

In our implementation, we calculate MAC_{CS} on a bin-by-bin basis for the appropriate refractive indices from Chang and Charalampopoulos (2006), as well as MAC_{CS} if all the coating thicknesses were zero, then sum both and divide the total coated absorption by the total uncoated absorption.

Comparing their data to the measurements by Liu et al. (2017), Wu et al. (2018) found agreement within $\sim 5\%$ for MAC at $532\ \text{nm}$, and $\sim 20\%$ for scattering at $1064\ \text{nm}$, however they also used a specific wavelength-dependent BC refractive index in this comparison. Again, as this parametrisation only gives E_{Abs}, we multiply the calculated E_{Abs} by MAC_{BB} to give the coated MAC.

The Chak-E_{Abs} and Chak-MAC parametrisations

Chakrabarty and Heinson (2018) developed a parametrisation applying discrete-dipole approximation calculations to simulated BC particles. Particles were generated in a similar manner as Wu et al. (2018). The parametrisation is described in several different forms, and here we apply two approaches, Chak-MAC and Chak-E_{Abs}. In Chak-MAC, MAC is calculated using

$$\text{MAC} = (3.6/\lambda) \left(\frac{M_{\text{tot}}}{M_{\text{BC}}} \right)^{(1/3)},$$

where $M_{\text{tot}} = M_{\text{non-BC}} + M_{\text{BC}}$.

In Chak-E_{Abs}, E_{Abs} is calculated as

$$E_{\text{Abs}} = \left(\frac{M_{\text{tot}}}{M_{\text{BC}}} \right)^{(1/3)}.$$

We then multiply E_{Abs} by MAC_{BB} to calculate MAC. The implication of the comparison between Chak-E_{Abs} and Chak-MAC is that the MAC of uncoated BC follows the rule $\text{MAC}_{\text{bare}} = (3.6/\lambda)$, which produces results 13% lower than MAC_{BB}.

S2 Schematic overview of SP2 single-particle mixing state processing

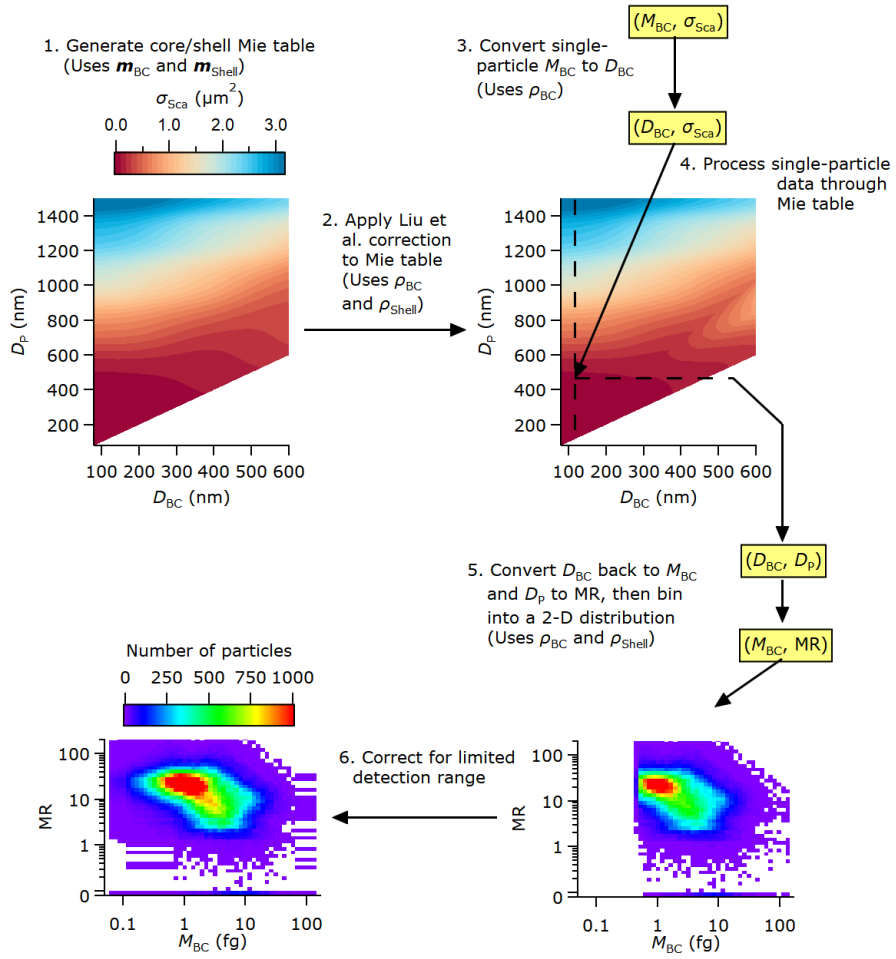

Figure S2. Schematic of the steps to generate 2-D distributions of MR versus M_{BC}. The steps are described in the text in Sect. 4.1.

~~S2~~ S3 Correction for SP2 limited detection range

Figure S3 shows BC properties from one straight and level run on the 4 September 2017 (shown in Fig. 5, though equivalent distributions were generated for each straight and level run during the campaign. Panel (a) shows the number mass distributions of BC cores. We do not ~~correc~~ correct for particles with BC content that is too small for the instrument to detect as these particles contain only a small fraction of the total BC mass concentration (Laborde et al., 2012b). Figure S3 (a) shows two distributions- one for all detected particles, and another for those that had a successful leading-edge only (LEO) fit to measure the scattering cross-section of BC-containing particles at 1064 nm. Of the particles that are detected, not all of them have a successful LEO fit due to the limited detection range of the scattering channel, as well as the relative importance of detector noise and saturation for different sized particles. The size-dependent ratio of these two distributions (F_{LEO}) is shown as the black line in panel (b). For most of the BC size distribution F_{LEO} was around 70 – 80 %, decreasing sharply to zero below 0.5 fg M_{BC} at the low end, and gradually decreasing from 0.8 to ~0.5 above around 10 fg, though this high end was noisy due to limited particles at the larger sizes.

Figure S3 (b) also shows the distribution of E_{Sca} versus M_{BC}, where E_{Sca} is the ratio of the measured scattering cross-section to Mie calculations for a bare BC core. E_{Sca} is a useful diagnostic as it gives an indication of BC mixing state that is independent of the morphology of the mixed particle. It is also unconstrained by the physical impossibility of concepts such as negative coating thickness, which arise due to the particle-by-particle variability of the measured signals. This plot shows a distribution of E_{Sca} around 100 for a 1 fg core, decreasing with size by an order of magnitude up to cores around 4 fg. There were few particles measured with E_{Sca} around 1, for bare BC cores, suggesting almost all the BC-containing particles had some degree of internal mixing. At the high and low ends of the M_{BC} distribution, where F_{LEO} dropped below 0.5, the MR distributions of the neighbouring bins were extended to complete the distribution, in proportion to the number of particles measured.

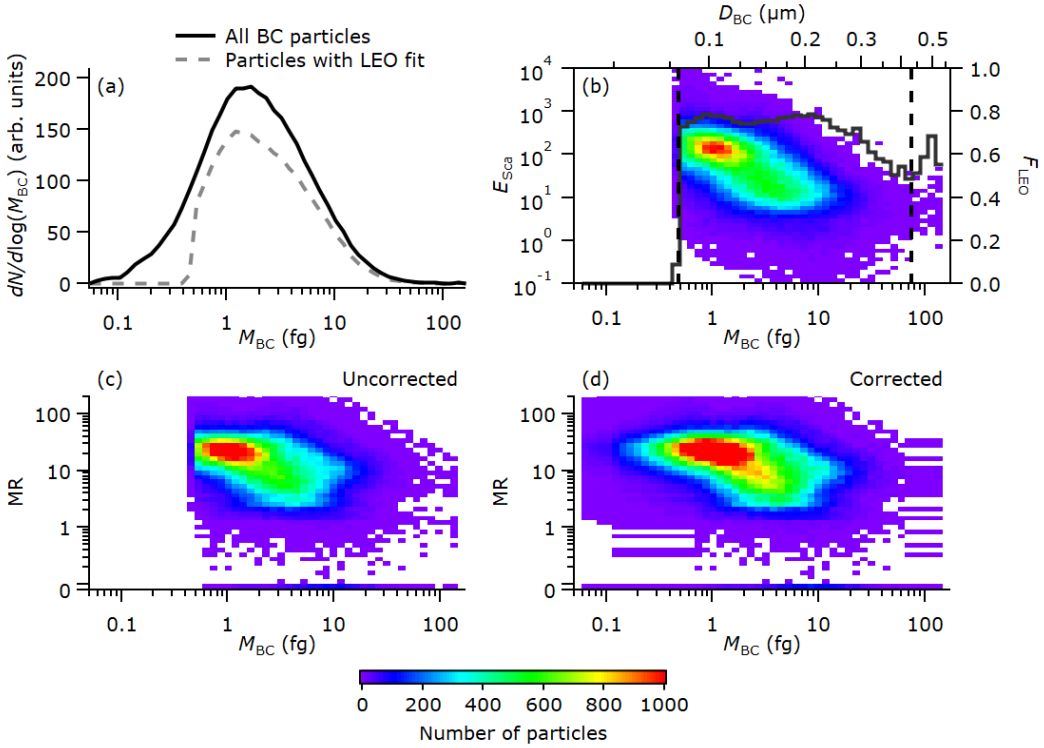

Figure S3. Panel (a) shows the number distribution of BC cores, both for all particles and just those with a good LEO fit. Panel (b) shows the distribution of E_{Sca} for particles of different M_{BC}, and the fraction of particles with a good LEO fit at each size. The vertical dashed lines show the bounds of the region where F_{LEO} was above 0.5. Panels (c) and (d) show the 2-D distributions of BC size and mixing state, comparing the distributions before and after correction for the limited detection of particles by the SP2 instrument.

~~S3~~ S4 Monte-Carlo uncertainty analysis in Mie models

The aim of this Monte-Carlo uncertainty analysis is to determine the uncertainty of parameters such as coating thickness, MAC, and AAE, that are derived using the optical codes described in Sect. S1. These uncertainties cannot be determined analytically due to the complexity of the calculation. Our approach is to use the uncertainty in the input variables to generate a scale factor (κ) to represent the variability that each input variable might have if it were measured a large number of times, in this case 10000. Arrays of scale factors were generated such that the distribution of each scale factor is a Gaussian distribution centred on one, with a width of the stated uncertainty for each variable. For example, to represent the 11% uncertainty in the SP2 scattering channel, the scale factor array is made of 10000 normally distributed numbers with a mean of 1 and a standard deviation of 0.11. For each calculation, this was then used to multiply the calibration factor for the SP2 scattering channel.

The variables we considered in this analysis are the calibrations for the SP2's incandescence and scattering channels, and the concentrations of the species measured by the AMS, which are used to calculate the density and refractive index of the coatings. We do not consider the density and refractive index of the BC in these calculations. For the purposes of the inversion to determine the BC properties based on the SP2 data, the values of $\rho_{\mathrm{BC}} = 1.8\ \mathrm{g\,cm^{-3}}$ and $\boldsymbol{m}_{\mathrm{BC}} = (2.26 - 1.26i)$ are used for the reasons given in Sect. 4.1. Particularly when using the Liu et al. (2017) parametrisation, these are not free parameters, and previous literature provides little guidance as to what the uncertainty is on these parameters. During the forward model calculations of MAC and AAE, our analysis explicitly includes different values of $\boldsymbol{m}_{\mathrm{BC}}$.

Scale factors were applied for the SP2 and AMS data from one straight and level run from the aircraft measurements on 1st September. This run was chosen as it was relatively short (4 minutes) so the calculation is quicker to run.

SP2 calibrations

The SP2's scattering channel was calibrated using nebulised 200 nm PSLs, and the measured modal signal varied by $\pm 11\%$ throughout the campaign. The incandescence channel is used to determine single particle BC mass, and this channel was calibrated using nebulised Aquadag, which was selected by mass using a centrifugal particle mass ~~analyzer~~ analyser (CPMA), and corrected as described by Laborde et al. (2012b). The uncertainty in this incandescence calibration is largely determined by the varying sensitivity of the instrument to different types of BC, which is around $\pm$ 14% (Laborde et al., 2012a). Laborde et al. (2012b) also showed that a 9% uncertainty in the accuracy of any individual incandescence calibration is reasonable, based on multiple calibrations with multiple instruments. The uncertainty in the mass and scattering cross-section of any individual particle is larger than these numbers, but this only serves to widen the measured distributions and has a minimal impact on the average properties of the particles or the integrated distributions.

AMS concentrations

The AMS chemical species measurements are used to calculate the density and refractive index of the BC coatings. The concentration, C_{S}, of a species, S, measured by the AMS scales with calibration factors described by Canagaratna et al. (2007):

$$C_{\mathrm{S}} \propto \frac{1}{\mathrm{IE_{NO3}}} \frac{1}{\mathrm{RIE_S}} \frac{1}{\mathrm{CE}} \frac{1}{Q},$$

where $\mathrm{IE_{NO3}}$ is the ionisation efficiency of $\mathrm{NO_3}$, $\mathrm{RIE_S}$ is the relative ionisation efficiency of the species in question, CE is the collection efficiency, and Q is the flowrate.

Bahreini et al. (2009) summarised the uncertainties associated with these factors based on previous literature available at the time. It is conventional in the AMS community to quote 2-σ uncertainties, so the standard deviation is half these values. The 2-σ uncertainties on $\mathrm{IE_{NO3}}$ and $\mathrm{RIE_{NH_4}}$ are both $\sim 10\%$, taken from the ammonium nitrate calibrations. The 2-σ uncertainties on $\mathrm{RIE_{SO_4}}$ and $\mathrm{RIE_{OA}}$ are 15% and 20%. As we have used the composition-dependent parametrisation to calculate CE (Middlebrook et al., 2012), the 2-σ uncertainty on CE is around 30%. The scale factors for each species are then

$$\kappa_{\mathrm{NO_3}} = \kappa_{\mathrm{IE_{NO3}}} \times \kappa_{\mathrm{CE}} \times \kappa_{\mathrm{TE}}$$

$$\kappa_{\mathrm{OA}} = \kappa_{\mathrm{IE_{NO_3}}} \times \kappa_{\mathrm{RIE_{OA}}} \times \kappa_{\mathrm{CE}} \times \kappa_{\mathrm{TE}}$$

$$\kappa_{\mathrm{SO_4}} = \kappa_{\mathrm{IE_{NO_3}}} \times \kappa_{\mathrm{RIE_{SO_4}}} \times \kappa_{\mathrm{CE}} \times \kappa_{\mathrm{TE}}$$

$$\kappa_{\mathrm{NH_4}} = \kappa_{\mathrm{IE_{NO_3}}} \times \kappa_{\mathrm{RIE_{NH_4}}} \times \kappa_{\mathrm{CE}} \times \kappa_{\mathrm{TE}}$$

Using this method, the resultant 2-σ uncertainties on $\mathrm{NO_3}$, OA, $\mathrm{SO_4}$ and $\mathrm{NH_4}$ mass concentrations are 33%, 39%, 37% and 36% respectively, which compare well to the numbers provided by Bahreini et al. (2009).

Assumed properties of organic aerosol

The composition-dependent calculations of the coating density and refractive index require knowledge of the properties of the aerosol components. For inorganic aerosol these are fairly well known, but the variable composition of OA means its properties can vary. For density we use the values determined by Cross et al. (2007) of 1.77 $\mathrm{g\,cm^{-3}}$ for inorganics and 1.2 $\mathrm{g\,cm^{-3}}$ for organics. These values were successfully used by Cross et al. (2007) in a comparison of light scattering to aerodynamic size using the AMS composition to calculate density. The uncertainty in the OA density is not immediately obvious, but a value of ± 0.1 $\mathrm{g\,cm^{-3}}$ seems appropriate based on previous literature (e.g. Kroll et al., 2009).

For the coating refractive index, we use a top-down approach. Previous work has often used a value of $1.5+0i$ (e.g. Schwarz et al., 2008; Taylor et al., 2015; Liu et al., 2015, 2017), and Taylor et al. (2015) also showed that this is a small sensitivity to the determination of particle size. Assuming a 9% BC mass fraction of the total submicron aerosol (Wu et al., 2020), volume mixing assuming $\boldsymbol{m}_{\mathrm{BC}} = 1.85-0.71i$ then gives an effective refractive index with a real component of 1.53. This value compares well with previous estimates by Haywood et al. (2003) and Peers et al. (2019), who found 1.54 and 1.51 respectively by comparing to bulk optical measurements. Comparing to the range of effective refractive index values found in previous studies of biomass burning (Guyon et al., 2003; Sayer et al., 2014), an uncertainty in the real component of the coating refractive index of 0.04 is a good conservative estimate.

Monte Carlo Results

Table S2 shows the results of the Monte Carlo analysis in terms of physical properties of the particles. The uncertainties in the derived coating thicknesses are around $\pm 8\%$. A comparison by Laborde et al. (2012b) showed that the whole range from different SP2 instruments was contained within $\pm 17\%$, which could be considered representative of a 2-σ uncertainty, and so compares very well with our estimate. The uncertainty in MR is larger, probably due to the uncertainty in the coating density.

Table S2. Mean and standard deviation of physical parameters involved in the Monte Carlo analysis of different optical models.

	Mean	**Standard deviation**
Median shell/core diameter ratio	2.33	0.15
Median MR	8.7	1.8
Median coating thickness (nm)	86	7

Table S3 shows the outputs of the Monte Carlo analysis. For the output of the optical models in terms of MAC and AAE, the derived uncertainties are in the range 2 – 12%. We suspect that, when using a polydisperse BC distribution, competing effects of varying the input parameters cancel out, reducing the uncertainty of the optical properties compared to the physical properties.

Table S3. Monte Carlo relative standard deviations of bulk absorption parameters using different optical schemes. For the optical models that have a dependence on $\boldsymbol{m}_{\mathrm{BC}}$ (Core/shell, CS-E_{Abs} volume mixing, Maxwell-Garnett and Bruggemann), the average value is listed here.

	Core/shell	CS-E_{Abs}	Volume mixing	Maxwell-Garnett	Bruggemann	Liu-$E_{\mathrm{Abs/Sca}}$	Chak-MAC	Chak-E_{Abs}	Wu-E_{Abs}
MAC 405 nm	0.07	0.04	0.12	0.12	0.12	0.04	0.07	0.07	0.03
MAC 514 nm	0.06	0.04	0.11	0.11	0.11	0.05	0.07	0.07	0.04
MAC 655 nm	0.05	0.05	0.11	0.11	0.11	0.05	0.07	0.07	0.04
AAE~~405/514~~405–514	0.09	0.03	0.09	0.09	0.09	0.03	0	0	0.03
AAE~~514/655~~514–655	0.07	0.03	0.07	0.07	0.07	0.02	0	0	0.03

~~S4~~ S5 Skin-depth shielding in Mie models

In the geometric optics regime, the absorption cross-section of a black sphere is the same as its geometric cross-section, πr^2, where r is the radius. This cross-section is independent of wavelength. In Mie theory, absorbing spheres asymptote to the geometric optics regime when they are sufficiently large and sufficiently absorbing. A useful concept to illustrate this transition is the optical skin depth, defined as $\delta = \lambda/(2\pi k_{\mathrm{BC}})$ (Hecht, 2014), where k_{BC} is the imaginary component of $\boldsymbol{m}_{\mathrm{BC}}$. This is the distance over which the intensity of light penetrating an absorbing medium drops by a factor of $1/e$. For clarity, this skin depth is not related to coatings in the core/shell model- it is simply the part of a homogeneous absorbing sphere that is near the surface. For small spheres the skin depth is not an issue, but when they become similar in ~~size~~ radius to the skin depth, the centre of the sphere is essentially shielded by the surface, and is therefore less effective at absorbing incident light. When the sphere becomes large enough, the centre receives little to no light, and only the region near the surface of the particle is able to absorb light. The absorption therefore scales with cross-section rather than volume, and the MAC scales inversely with diameter. This 'skin-depth shielding' is strongest for larger particles, high values of k_{BC}, and shorter wavelengths.

This wavelength dependence causes the underprediction of MAC for the core/shell Mie model in Fig. 6 at 405 nm, but not at longer wavelengths. Figure S5 shows example calculations of MAC for uncoated BC particles, as well as coated. Particles with BC cores of 185 nm (the average MMD measured during CLARIFY) fall within the geometric optics regime at a wavelength of 405 nm, but not at 655 nm. Therefore, for this size of particle, the skin-depth shielding reduces the blue MAC but not the red. The presence of coatings modifies the shape and magnitude of the MAC curves in Fig. S5, but it does not change the overall concept. These calculations were carried out with nonabsorbing coatings, confirming that this is an effect of Mie theory and not related to BrC. The wavelength dependence of the skin-depth shielding is the reason the Mie calculations have AAE values below 1 (shown in Fig. 7), and the stronger effect at higher values of k_{BC} causes a lower AAE.

~~S5 Impact of m_{BC} on MAC for typical particles~~

~~Figure 8 shows core/shell MAC and AAE calculations with core and shell diameters calculated using typical core/shell particles; the D_C distribution taken from Fig. 5a, and representative shell/core ratios of 2.4. Example $\boldsymbol{m}_{\mathrm{BC}}$ values follow the rule of $n_{\mathrm{BC}} = k_{\mathrm{BC}} + 1$, where n_{BC} and k_{BC} are the real and imaginary components of $\boldsymbol{m}_{\mathrm{BC}}$. A value of 1.5 - 0i was also used for the shell refractive index. This figure is discussed further in Sect. 5.2.~~

~~MAC and AAE as a function of $\boldsymbol{m}_{\mathrm{BC}}$ for typical core/shell particles measured during CLARIFY.~~

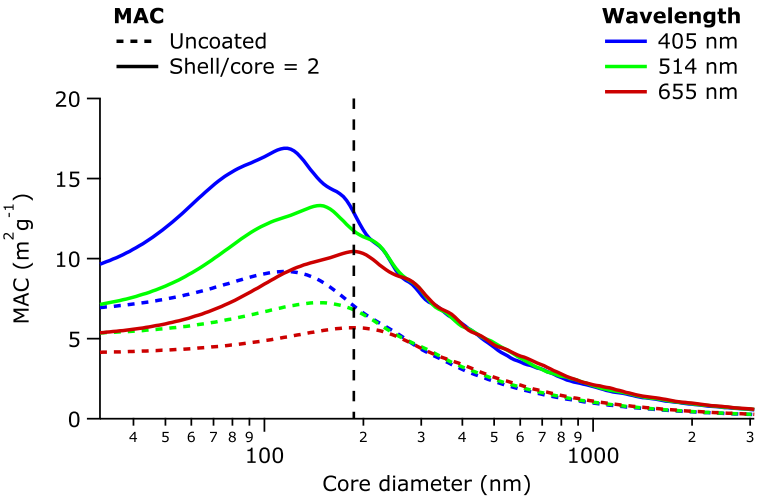

Figure S5. MAC for different core diameters, using the Mie core/shell model. Calculations were performed using $\boldsymbol{m}_{\mathrm{BC}} = (1.85 - 0.71)i$. The vertical dashed line is at 185 nm, which is similar to the average MMD in CLARIFY shown in Fig. 3.